2004-09

Inlet distortion generation for a transonic compressor

Papamarkos, Ioannis.

Monterey, California. Naval Postgraduate School

NAVAL POSTGRADUATE SCHOOL

MONTEREY, CALIFORNIA

THESIS

INLET DISTORTION GENERATION FOR A TRANSONIC COMPRESSOR

by

Ioannis Papamarkos

September 2004

Thesis Advisor: Raymond Shreeve
Second Reader: Garth Hobson

Approved for public release; distribution is unlimited.

THIS PAGE INTENTIONALLY LEFT BLANK

REPORT DOCUMENTATION PAGE			Form Approved OMB No. 0704-0188
Public reporting burden for this collection of information is estimated to average 1 hour per response, including the time for reviewing instruction, searching existing data sources, gathering and maintaining the data needed, and completing and reviewing the collection of information. Send comments regarding this burden estimate or any other aspect of this collection of information, including suggestions for reducing this burden, to Washington headquarters Services, Directorate for Information Operations and Reports, 1215 Jefferson Davis Highway, Suite 1204, Arlington, VA 22202-4302, and to the Office of Management and Budget, Paperwork Reduction Project (0704-0188) Washington DC 20503.			
1. AGENCY USE ONLY ***(Leave blank)***	**2. REPORT DATE** September 2004	**3. REPORT TYPE AND DATES COVERED** Master's Thesis	
4. TITLE AND SUBTITLE: Inlet Distortion Generation for a Transonic Compressor			**5. FUNDING NUMBERS**
6. AUTHOR(S) Ioannis Papamarkos			
7. PERFORMING ORGANIZATION NAME(S) AND ADDRESS(ES) Naval Postgraduate School Monterey, CA 93943-5000			**8. PERFORMING ORGANIZATION REPORT NUMBER**
9. SPONSORING /MONITORING AGENCY NAME(S) AND ADDRESS(ES)			**10. SPONSORING/MONITORING AGENCY REPORT NUMBER**
11. SUPPLEMENTARY NOTES The views expressed in this thesis are those of the author and do not reflect the official policy or position of the Department of Defense or the U.S. Government.			
12a. DISTRIBUTION / AVAILABILITY STATEMENT Approved for public release; distribution is unlimited.			**12b. DISTRIBUTION CODE**

13. ABSTRACT ***(maximum 200 words)***

A single-stage transonic research compressor and test rig are to be used to obtain data on the effect of inlet flow distortion on compressor (and therefore engine) stall. Auxiliary injection was examined as a technique for generating distortion in inlet stagnation pressure, or temperature, or to simulate the more complex effects of engine steam ingestion from a catapult launch. Engineering analyses were developed and programmed in EES to relate inlet conditions to the compressor characteristics, for both pressure and temperature distortion. An injection duct area of 8% was selected to limit the required heater power. A CFD analysis was carried out to predict the compressor inlet flow field and hence position the injection duct exit. It was found that a broad range of distortion parameters could be generated by simply ducting (and heating) atmospheric air (or steam) through an auxiliary inlet throttle valve.

14. SUBJECT TERMS Compressor stall, Inlet distortion, Transonic compressor test.			**15. NUMBER OF PAGES** 72
			16. PRICE CODE
17. SECURITY CLASSIFICATION OF REPORT Unclassified	**18. SECURITY CLASSIFICATION OF THIS PAGE** Unclassified	**19. SECURITY CLASSIFICATION OF ABSTRACT** Unclassified	**20. LIMITATION OF ABSTRACT** UL

NSN 7540-01-280-5500

Standard Form 298 (Rev. 2-89)
Prescribed by ANSI Std. 239-18

THIS PAGE INTENTIONALLY LEFT BLANK

Approved for public release; distribution is unlimited

INLET DISTORTION GENERATION FOR A TRANSONIC COMPRESSOR

Ioannis Papamarkos
Lieutenant, Hellenic Navy
B.S Hellenic Naval Academy, 1995

Submitted in partial fulfillment of the
requirements for the degree of

MASTER OF SCIENCE IN MECHANICAL ENGINEERING

from the

NAVAL POSTGRADUATE SCHOOL
September 2004

Author:

Ioannis Papamarkos

Approved by:

Raymond Shreeve
Thesis Advisor

Garth Hobson
Second Reader

Anthony J. Healey
Chairman, Department of Mechanical and Astronautical Engineering

THIS PAGE INTENTIONALLY LEFT BLANK

ABSTRACT

A single-stage transonic research compressor and test rig are to be used to obtain data on the effect of inlet flow distortion on compressor (and therefore engine) stall. Auxiliary injection was examined as a technique for generating distortion in inlet stagnation pressure, or temperature, or to simulate the more complex effects of engine steam ingestion from a catapult launch. Engineering analyses were developed and programmed in EES to relate inlet conditions to the compressor characteristics, for both pressure and temperature distortion. An injection duct area of 8% was selected to limit the required heater power. A CFD analysis was carried out to predict the compressor inlet flow field and hence position the injection duct exit. It was found that a broad range of distortion parameters could be generated by simply ducting (and heating) atmospheric air (or steam) through an auxiliary inlet throttle valve.

THIS PAGE INTENTIONALLY LEFT BLANK

TABLE OF CONTENTS

I. INTRODUCTION 1

II. COMPRESSOR AND INLET GEOMETRY 3
- A. FACILITY AND OPERATION 3
- B. TRANSONIC COMPRESSOR 5
- C. COMPRESSOR PERFORMANCE MAP 5
- D. DISTORTION GENERATION CONCEPT 6

III. ANALYSIS OF AUXILIARY INJECTION 9
- A. GEOMETRY AND NOTATION 9
- B. PRESSURE DISTORTION GENERATION 10
  - 1. Analysis 10
  - 2. Results 13
- C. TEMPERATURE DISTORTION GENERATION 17
  - 1. Analysis 17
  - 2. Results 19

IV. COMPUTATIONAL ANALYSIS OF DISTORTION GENERATION 23
- A. PRESSURE DISTORTION 27
- B. TEMPERATURE DISTORTION 28
- C. GRID SENSITIVITY 30

V. CONCLUSIONS AND RECOMMENDATIONS 33

APPENDIX A TEST AND INLET DISTORTION DATA 35
- A. EXPERIMENTAL PERFORMANCE MAP 35
- B. PRESSURE DISTORTION 36
- C. TEMPERATURE DISTORTION 37

APPENDIX B MASS FLOW RATE EQUATION 39

APPENDIX C PRESSURE DISTORTION (EES CODE) 41

APPENDIX D TEMPERATURE DISTORTION (EES CODE) 47

APPENDIX E INLET VELOCITY RATIO 51
- A. PRESSURE DISTORTION 51
- B. TEMPERATURE DISTORTION 51

LIST OF REFERENCES 53

INITIAL DISTRIBUTION LIST 55

THIS PAGE INTENTIONALLY LEFT BLANK

LIST OF FIGURES

Figure 1. Schematic diagram of the transonic compressor test rig (from O'Brian, 2000) 4
Figure 2. Transonic single stage compressor 5
Figure 3. Experimental compressor performance (without inlet distortion) 6
Figure 4. Auxiliary injection concept for generating controlled inlet distortion..... 7
Figure 5. Schematic representation of the distortion generation by secondary flow injection..... 9
Figure 6. Compressor pumping characteristic measured at 90% design speed and degradation assumed for distortion design. 14
Figure 7. Mach number variation with pressure distortion parameter π (α=0.08, $\nu = 1.05$)..... 15
Figure 8. Injection stagnation pressure variation with distortion parameter π (α=0.08, $\nu = 1.05$)..... 15
Figure 9. Mass flow-rate variation with distortion parameter (α=0.08, ν=1.05) 16
Figure 10. Mach number variation with temperature distortion parameter τ (α=0.08, ν=1.05)..... 20
Figure 11. Energy required to heat the injected flow (α=0.08, ν=1.05)..... 20
Figure 12. Mass flow-rate variation with distortion parameter τ (α=0.08, ν=1.05)..... 21
Figure 13. Injected flow area..... 23
Figure 14. Geometry of the duct used in CFD ACE code..... 24
Figure 15. Example of the grid used to calculate the mixing from auxiliary injection.... 25
Figure 16. Inlet to exit flow and lines chosen at the exit for data comparison..... 26
Figure 17. Locations that were selected at the exit plane (station 4) to compare results. 26
Figure 18. Stagnation pressure distribution at station 4 (at Z = 0.044 m) for different inlet duct lengths (90% speed, π = 1.05, τ = 1) 27
Figure 19. Stagnation pressure distribution at station 4 (at Y = 0.115 m) for different inlet duct lengths (90% speed, π = 1.05, τ = 1) 28
Figure 20. Stagnation temperature distribution at station 4 (at Z = 0.044 m) for different inlet duct lengths (90% speed, π = 1.0, τ = 1.25)..... 29
Figure 21. Stagnation temperature distribution at station 4 (at Y = 0.115 m) for different inlet duct lengths (90% speed, π = 1.0, τ = 1.25)..... 29
Figure 22. Stagnation pressure distribution at station 4 (at Z = 0.044 m) for different grid selection (90% speed, π = 1.05, τ = 1) 31
Figure 23. Stagnation pressure distribution at station 4 (at Y = 0.115 m) for different grid selection (90% speed, π = 1.05, τ = 1) 31
Figure 24. Stagnation temperature distribution at station 4 (at Y = 0.115 m) for different grid selection (90% speed, π = 1.0, τ = 1.25)..... 32
Figure 25. Stagnation temperature distribution at station 4 (at Z = 0.044 m) for different grid selection (90% speed, π = 1.0, τ = 1.25)..... 32

THIS PAGE INTENTIONALLY LEFT BLANK

LIST OF TABLES

Table 1. 80% operational speed data 35
Table 2. 90% operational speed data 35
Table 3. 100% operational speed data 36
Table 4. Mass flow vs. pressure ratio p..... 37
Table 5. Mach number vs pressure ratio p 37
Table 6. Injected flow stagnation pressure vs. pressure ratio p 37
Table 7. Mass flow vs. temperature ratio t..... 37
Table 8. Mach number vs. temperature ratio t 38
Table 9. Heat transfer to the injected flow vs. temperature ratio t..... 38

THIS PAGE INTENTIONALLY LEFT BLANK

ACKNOWLEDGMENTS

Many thanks to my Professors, Raymond Shreeve and Garth Hobson for their support. Also, many thanks to Anthony Gannon and the personnel of the NPS Turbopropulsion Laboratory, John Gibson, Rick Still and Doug Seivwright.

THIS PAGE INTENTIONALLY LEFT BLANK

I. INTRODUCTION

Engines for military fighter aircraft must be designed to operate stably over a required flight envelope. An adequate “stall margin” is usually an engine design requirement. Since distortion of the flow into the fan or compressor is known to reduce the stall margin, stable operation with a specified level of inlet distortion (due to imperfect flow through the inlet) is also usually specified as a design requirement.

The joint strike fighter (JSF) faces two other potential inlet distortion problems, - gas re-ingestion due to jet deflection, and steam ingestion on carrier take-off. The potential problem of gas re-ingestion of the STOVL version in hover was lessened by the selection of the lift-fan over the jet-lift concept, but the potential for an engine stall on carrier take-off must be addressed in view of the single-engine aircraft design. In an effort to understand the temperature variation due to steam ingestion during the catapult launch, the JSF program office recently conducted a series of tests to survey the temperature field and the location of steam exiting a catapult during launch (Donelson S., Briggs T., 2003). However, at the current time, steam ingestion from an aircraft carrier’s catapult is one of the least understood potential mechanisms for engine stall.

Most concentration has been placed previously on pressure distortion (produced by inlet separations), and temperature distortion (from engine gas re-ingestion). The Society of Automotive Engineers (SAE) addressed the aircraft engine-airframe compatibility development process, how it was affected by flow distortion, and more particularly how to analyze the inlet total pressure distortion effects on gas turbine engines (SAE – AIR 1419, 1983). Also, the SAE S-16 committee reported tests to examine temperature distortion effects on the intake/engine aerodynamic compatibility, and their impact on the design and development of aircraft propulsion systems. Engine performance degradation, including power loss due to the compressor instability, has been attributed to engine inlet total temperature distortion (SAE ARD50015, 1991).

The overall goal of the present study is to help develop and validate methods that can predict the effects of inlet flow distortion on the fan and compressor, and therefore engine, stability. It is clear that the analysis of the aerodynamic response of transonic

compressors and engines to non-uniform inlet flow is extremely complex. Consequently, if successful methods are to be developed, it is necessary also to conduct controlled experiments with distortion, to generate and measure controlled non-uniformity in both pressure and temperature into the fan or compressor, and obtain validation data for the prediction of instability and stall.

The need for detailed validation data motivated the present effort, which was to design an inlet distortion generation arrangement for the Naval Postgraduate School's transonic compressor test rig. This unique rig, incorporating a throttled inlet flow, allowed a somewhat unusual approach to be taken to the generation of distortion, one that would allow control of the degree of distortion, whether it was due to air stagnation pressure or temperature, or due to steam. The basic idea was to introduce a secondary flow with higher stagnation temperature, higher or lower stagnation pressure, or containing steam, into the flow entering the compressor. The design process required identifying a conceptual arrangement for the generation, developing an analysis of parallel-flow compressible mixing, which allowed the specification of the fully mixed-out condition, and the computational prediction of the mixing flow after the size of the injection duct had been selected.

In documenting the design, the compressor rig and distortion generation concept are first described in Chapter II. The analysis of compressible mixing, given the ratio of stagnation pressures, or temperatures, in parallel streams, is then described in Chapter III. The unusual requirement here was to be able to specify a required value for the corrected flow rate and stagnation pressure after mixing (supplied to the test compressor). The analysis allowed the secondary flow duct area to be selected such that it could provide pressure or temperature distortion with acceptable auxiliary piping and heater power levels.

The results of analyzing the proposed arrangement using the CFD code ACE are then described and discussed in Chapter IV. Conclusions and recommendations are given in Chapter V.

II. COMPRESSOR AND INLET GEOMETRY

A. FACILITY AND OPERATION

A schematic diagram showing the Transonic Compressor Rig (TCR) in the high-speed building at the Turbopropulsion Laboratory (TPL) at NPS is shown in Figure 1 (O' Brien J.M., 2000). The test compressor is driven by two opposed rotor air turbine stages, supplied by a 12-stage Allis-Chalmers (AC) axial compressor. The AC compressor can supply air continuously at up to 300 KPa at flow rates up to nearly 5 Kilograms per second. Pressurized air from the compressor is fed through a motor driven valve into the turbine drive unit. The electric drive motor is manually adjusted to control the compressor speed.

The test compressor draws atmospheric air through a rotating-plate throttle valve into a one-meter diameter settling chamber. A 0.46-meter diameter pipe, 5 meters in length and containing a flow nozzle, connects the chamber to the test compressor. A smooth contraction is provided between the 0.46-meter inlet pipe and the 0.279-meter diameter compressor case wall. The flow enters axially into the test compressor rotor and then, after the stator, exits axially through a honeycomb flow straightener, as shown in Figure 2. Not shown in these figures are an additional 1 MPa compressor that supplies air to a balance piston located on the drive shaft, which controls the axial force on the bearings of the rotor; also, a smaller shop compressor that provides dry air for the bearing oil-mist lubrication system, and other instrument air requirements.

The Transonic Compressor Rig is operated under manual control from a protected control room outside the compressor test cell. Two electrically driven butterfly valves are used to adjust the speed of the turbine, while maintaining adequate flow through the AC compressor. The rotating plate throttle, which is hydraulically actuated using a solenoid valve, is used to set the desired flow rate through the test compressor. The air pressure to the balance piston is adjusted by adjusting the instrument air pressure to a pneumatic regulator. Hence the operator must adjust four different valves in order to set the

operating condition for a single point on a constant speed line of the compressor map. This is significant when the proposal is to add auxiliary injection, requiring a further additional valve.

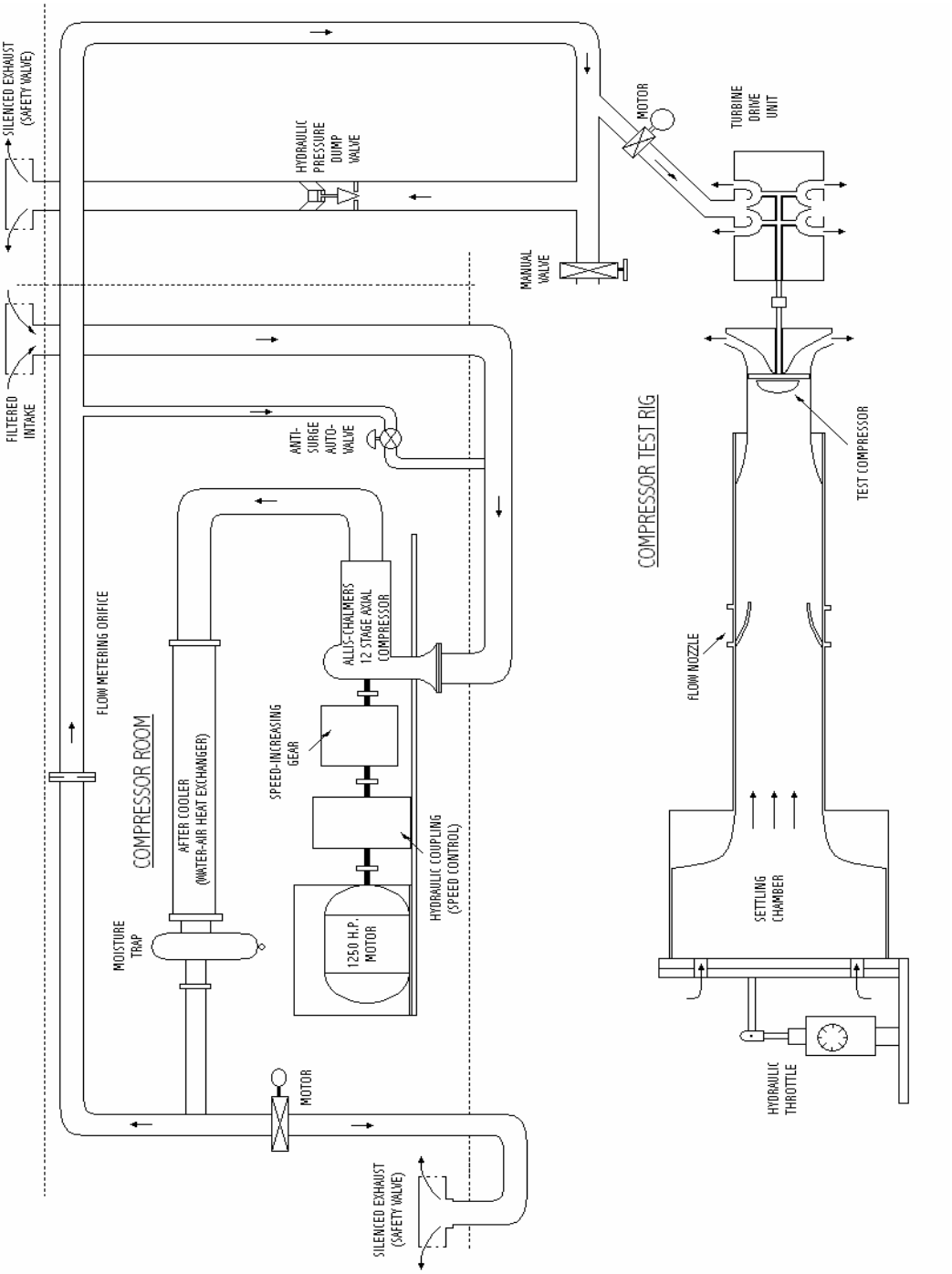

Figure 1. Schematic diagram of the transonic compressor test rig (from O'Brian, 2000)

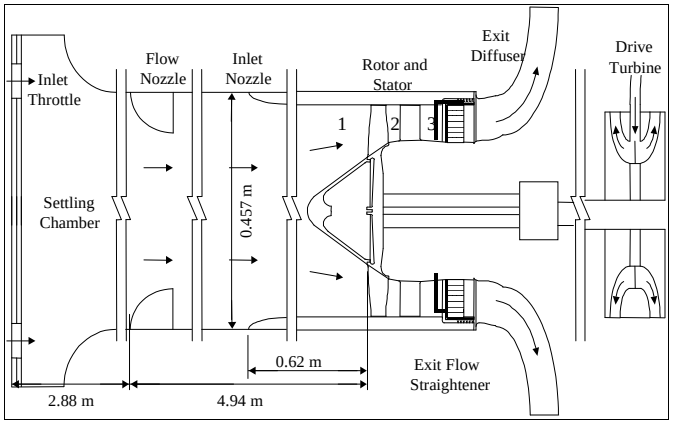

Figure 2. Transonic single stage compressor

B. TRANSONIC COMPRESSOR

The single stage transonic compressor was designed by Nelson L. Sanger at the NASA Glenn Research Center using CFD techniques (Sanger, 1996). The highly loaded design resulted in 22 blades in the rotor and 27 in the stator. The performance of the stage was mapped experimentally in the TCR (Gannon et al, 2004), and predicted using CFD codes (Hobson et al, 2004). Fixed instrumentation for performance mapping was installed at the three stations shown in Figure 2, and in the 0.279-meter diameter duct ahead of the rotor. It is significant to the present work that the case wall can be rotated to survey peripherally using fixed probes.

C. COMPRESSOR PERFORMANCE MAP

A performance test is usually conducted while maintaining a constant compressor speed. The test begins with the main throttle fully open. Data are then taken at various main throttle positions, giving desired increments in the flow rate. The stall boundary is established at low rotational speeds and is approached cautiously at near-design speeds. When stall does occur, it is necessary to open the throttle to restore stable operation, and possibly close it gradually again to more closely approach the stall boundary.

Performance map data are given Appendix A. (from Gannon, 2004) and data for 80 %, 90% and 100% of design speed are shown plotted in Figure 3. The data in Figure 3 represent the pumping characteristic of the installed Sanger stage when operating without distortion. It is likely that less pressure ratio will be produced at a given corrected flow

when distortion is introduced. This was considered in designing the auxiliary injection system to produce controlled distortion. The 90% speed line was used rather than the 100% speed line, and a 5% degradation in the pumped pressure was assumed at the compressor inlet.

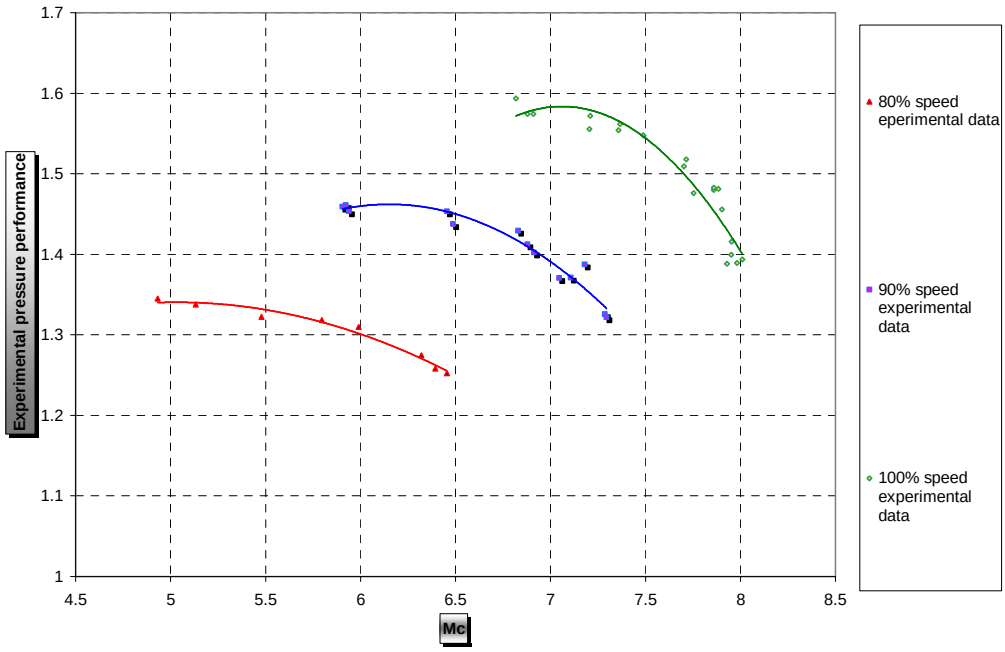

Figure 3. Experimental compressor performance (without inlet distortion)

D. DISTORTION GENERATION CONCEPT

Auxiliary injection into the inlet pipe, in order to generate controlled magnitudes of well-defined inlet distortion, is proposed. In order to avoid three-dimensional effects that would both complicate the prediction and require extensive inlet flow diagnostics, injection parallel with the main flow is proposed. A sketch of the conceptual arrangement is shown in Figure 4.

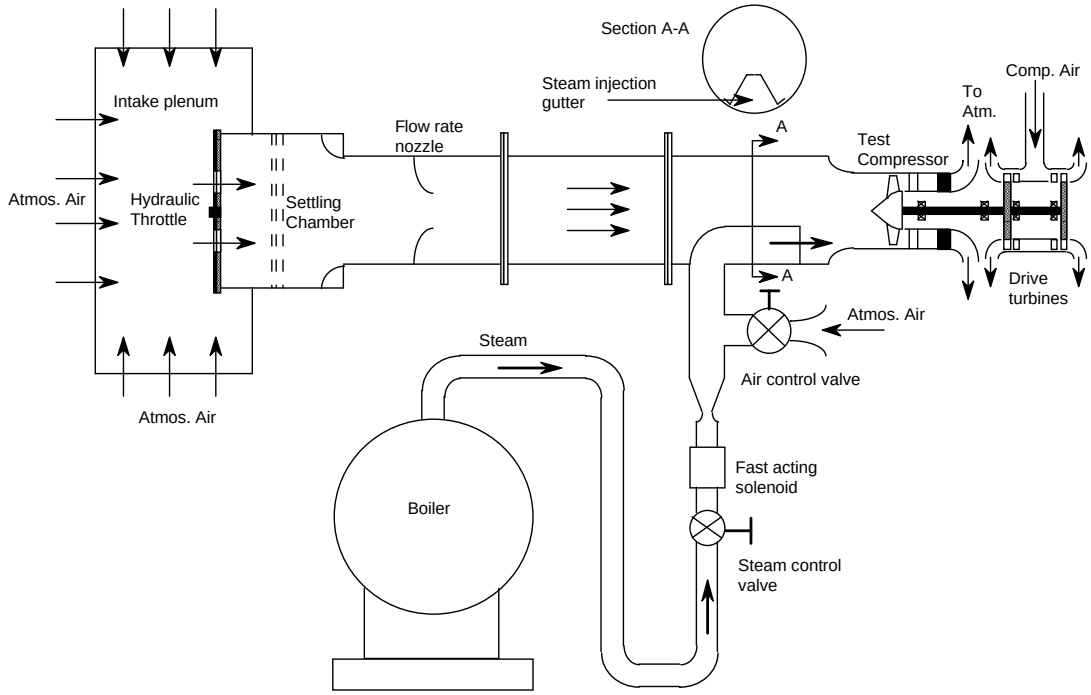

a) Conceptual arrangement

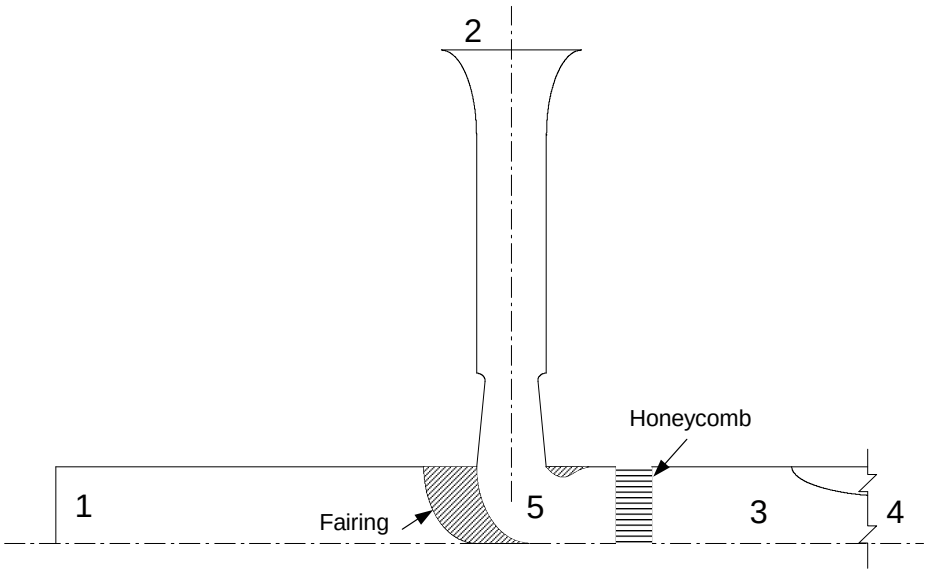

b) Duct detail

Figure 4. Auxiliary injection concept for generating controlled inlet distortion

THIS PAGE INTENTIONALLY LEFT BLANK

III. ANALYSIS OF AUXILIARY INJECTION

A. GEOMETRY AND NOTATION

Figure 5 shows the geometry that was used. Station 1 represents the main flow; station 2 represents the secondary or distorting flow; station 3 represents the end of the mixing of the main and secondary flows, and station 4 represents the entrance of the compressor.

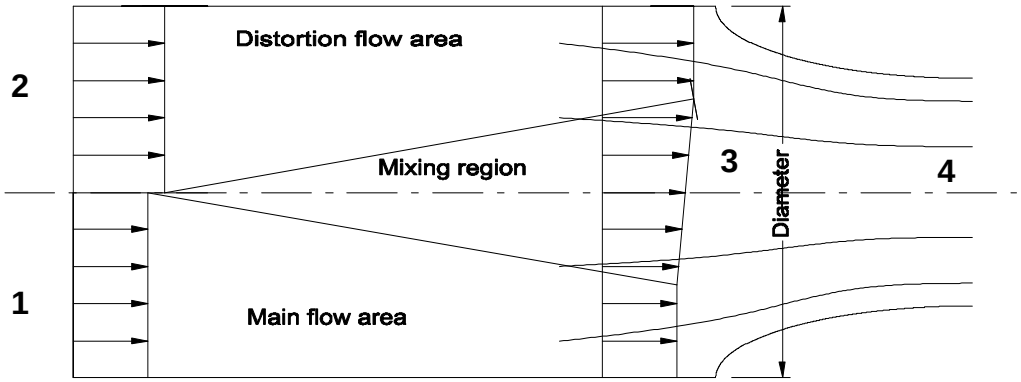

Figure 5. Schematic representation of the distortion generation by secondary flow injection

Notation:

M	Mach number
m	Mass flow rate
P	Pressure
Pt	Stagnation pressure
T	Temperature
Tt	Stagnation temperature
V	Velocity

R Gas constant

C_p Specific heat at constant pressure

C_v Specific heat at constant volume

γ Ratio of specific heats (here, γ=1.4)

α Ratio of secondary to overall flow area ($\alpha = \frac{A_2}{A_3}$)

π Ratio of secondary to main-flow stagnation pressure ($\pi = \frac{Pt_2}{Pt_1}$)

τ Ratio of secondary to main-flow stagnation temperature ($\tau = \frac{Tt_2}{Tt_1}$)

ν Ratio of stagnation pressure at station 3 to design value ($\nu = \frac{Pt_3}{Pt_{3d}}$)

Suffixes:

1 Main flow

2 Injected flow

3 Fully mixed-out flow (in inlet pipe)

4 Compressor inlet flow (after bell-mouth contraction)

d Design condition (no distortion)

std Standard atmosphere

B. PRESSURE DISTORTION GENERATION

1. Analysis

The following assumptions were made:

1. Neglect effect of friction at the wall
2. The two flows are at the same stagnation temperature (τ = 1)
3. After mixing, the flow is uniform at station 3.
4. The flow from station 3 to station 4 is isentropic ($Pt_3 = Pt_4$, $Tt_3 = Tt_4$)
5. The injected stream enters parallel to the main stream, so that $P_1 = P_2$.

It is assumed that Pt_3 is a fraction of Pt_{3d}, and that the fraction can be greater or less than unity (positive or negative pressure distortion). The goal is then to find the magnitude of Pt_2 which results in the required value of Pt_3.

Using conservation of mass

$$m_3 = m_2 + m_1 \tag{1}$$

From conservation of energy, in the absence of shaft work and heat addition, assuming a perfect gas,

$$m_3 Tt_3 = m_2 Tt_2 + m_1 Tt_1 \tag{2}$$

From conservation of momentum,

$$0 = m_1 V_1 + m_2 V_2 - m_3 V_3 + A_3 [P_1 - P_3] \tag{3}$$

The area ratio α, is given by, $\alpha = \frac{A_2}{A_3}$ (4)

and a value $0 < \alpha < 1$ is selected. The magnitude of the pressure distortion is defined as $\frac{Pt_2}{Pt_1} = \pi$. Both $\pi > 1$ and $\pi < 1$ are of interest.

The analytical approach followed was to express all the quantities with respect to the unknown Mach number at station 1 (M_1). The development is described as a series of steps:

1. Assume a value of Pt_3 / Pt_{3d}. The value of Pt_{3d} is taken from experimental data presented in Appendix A for 90% of the design of speed. The ratio is defined as

$$\frac{Pt_3}{Pt_{3d}} = \nu, \ (\nu < 1 \text{ or } > 1) \tag{6}$$

2. Evaluate Tt_3 from conservation of energy (equation 2) to obtain

$$Tt_3 = \frac{m_1 Tt_1 + m_2 Tt_2}{m_3} \tag{7}$$

Since $Tt_1 = Tt_2$, using equation (1),

$$Tt_1 = Tt_2 = Tt_3 \tag{8}$$

3. At any station, the flow rate can be expressed in terms of stagnation conditions and Mach numbers as in Appendix B.

$$m = \frac{Pt\mathrm{A}}{(\gamma RTt)^{0.5}} \gamma M \left(1 + \frac{(\gamma - 1)}{2} M^2\right)^{-\frac{(\gamma+1)}{2(\gamma-1)}} \tag{9}$$

Using the conventional (engine) notation, $\delta = \frac{Pt_3}{P_{std}}$, where P_{std} =standard atmosphere, $\delta_{31} = \frac{Pt_3}{Pt_1}$ is obtained using equation (9) and equation (1) as

$$\delta_{31} = \pi \left(\frac{A_2}{A_3}\right) M_2 \left(1 + \frac{(\gamma-1)}{2} M_2{}^2\right)^{-\frac{(\gamma+1)}{2(\gamma-1)}} + \frac{A_1}{A_3} M_1 \left(1 + \frac{(\gamma-1)}{2} M_1{}^2\right)^{-\frac{(\gamma+1)}{2(\gamma-1)}} \left[\frac{1}{M_3 \left(1 + \frac{(\gamma-1)}{2} M_3{}^2\right)}\right]^{-\frac{(\gamma+1)}{2(\gamma-1)}} \tag{10}$$

4. While Pt_2 is higher or lower than Pt_1, since both flows are subsonic $P_2 = P_1$. Therefore M_1 is different from M_2, but the two Mach numbers are related by

$$1 + \frac{(\gamma-1)}{2} M_2{}^2 = \left(1 + \frac{(\gamma-1)}{2} M_1{}^2\right) \pi^{\frac{(\gamma-1)}{\gamma}} \tag{11}$$

5. Finally, using equations (9) and (10) in equation (3) and introducing the relationships between velocity and Mach number, static and stagnation temperature, the following is obtained from the conservation of momentum,

$$0 = \delta_{31}\gamma\left(\frac{A_1}{A_3}\right)M_1{}^2\left(1+\frac{(\gamma-1)}{2}M_1{}^2\right)^{-\frac{(\gamma+1)}{2(\gamma-1)}}\left[1+\pi\frac{A_2}{A_1}\frac{M_2{}^2}{M_1{}^2}\left(\frac{2+(\gamma-1)M_2{}^2}{2+(\gamma-1)M_1{}^2}\right)^{-\frac{(\gamma+1)}{2(\gamma-1)}-0.5}\right]- \\ -\gamma M_3{}^2\left(1+\frac{(\gamma-1)}{2}M_3{}^2\right)^{-\frac{(\gamma+1)}{2(\gamma-1)}-0.5}+\left[\frac{\delta_{13}}{\left(1+\frac{(\gamma-1)}{2}M_1{}^2\right)^{\frac{\gamma}{(\gamma-1)}}}-\frac{1}{\left(1+\frac{(\gamma-1)}{2}M_3{}^2\right)^{\frac{\gamma}{(\gamma-1)}}}\right] \quad (12)$$

where $\delta_{13}=\frac{Pt_1}{Pt_3}$.

Equation (11) and equation (12) can be written as a single equation for one unknown Mach number. An EES code was written to solve first for M_1 and then M_2 and then calculate all the other unknowns (Appendix C).

2. Results

The inlet distortion design calculations were based on the assumption that $\frac{Pt_3}{Pt_{3d}}=\nu=1.05$ (that the compressor pumping capability would deteriorate with distortion present), and the corrected flow rate, $m_c=\frac{m\sqrt{T_t/T_{std}}}{P_t/P_{std}}$, would be given by the experimentally determined compressor map shown in Figure 3.

At 90% of the compressor design speed, the ratio of the inlet pressure to standard reference pressure measured in tests, with a second curve representing 5% deterioration, are shown in Figure 6. The unusual trend in the behavior of inlet pressure with throttling is the result of the throttle being in the inlet flow to the compressor. The upper curve was taken as the design curve for the distortion generation. Similar curves were calculated for 80% and 100% speed levels.

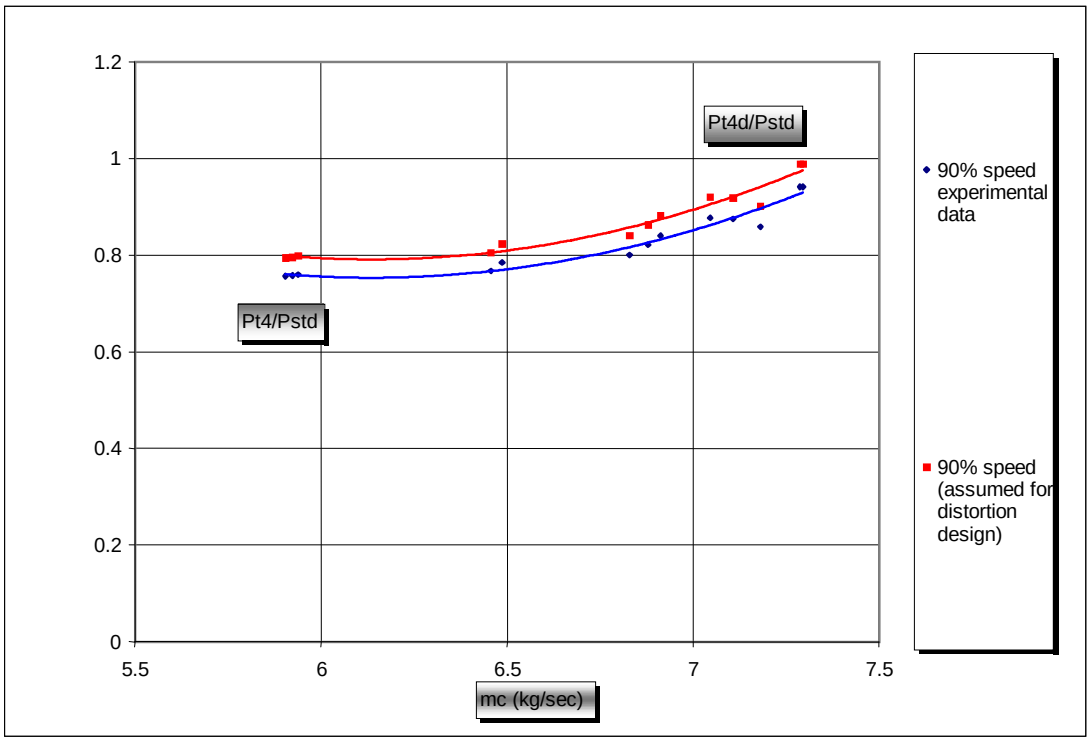

Figure 6. Compressor pumping characteristic measured at 90% design speed and degradation assumed for distortion design.

For reasons given in the following section, a design value of α=0.08 was selected. Calculations were then carried out for pressure distortion values of π from slightly smaller than unity to 1.05. Since the Mach number in the inlet pipe is very low, the ratio of the static to stagnation pressure (P_1/Pt_1) is very close to unity, and the minimum value of π (zero injection velocity) is, from Equation 7 of Appendix E, π=0.9965. Hence the full range of 'negative pressure distortion' is achieved by varying π only a fraction of a percent below unity. Similarly, the complete range of interest for 'positive pressure distortion' is achieved in the range $1<\pi<1.05$. Since little information is lost by the omission, only the results for $\pi > 1$ are shown plotted in the results.

The results are given in Figures 7-9 for operation at 80%, 90% and 100% of design speed. The Mach numbers in the main and secondary streams are shown in Figure 7, the stagnation pressures at stations 1 and 2, required to satisfy $Pt_3 = 1.05\, Pt_{3d}$, are shown in Figure 8, and the mass flow rates in the two streams are shown in Figure 9.

Note that all the blue curves are for the near-stall corrected mass flow at 90% operational speed.

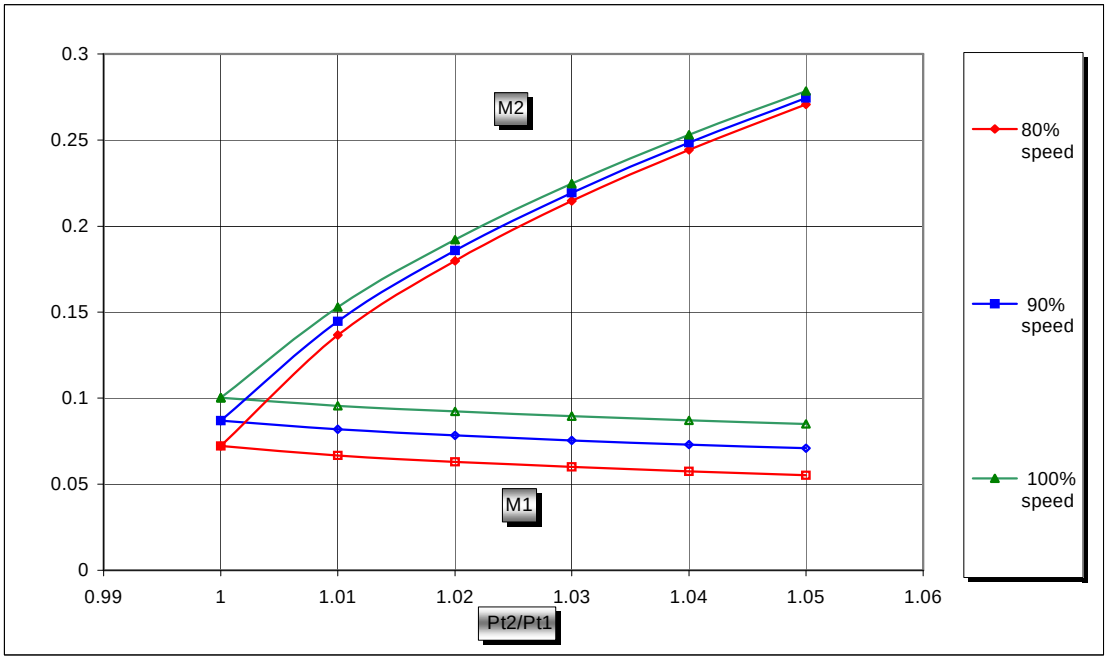

Figure 7. Mach number variation with pressure distortion parameter π (α =0.08, $\nu = 1.05$)

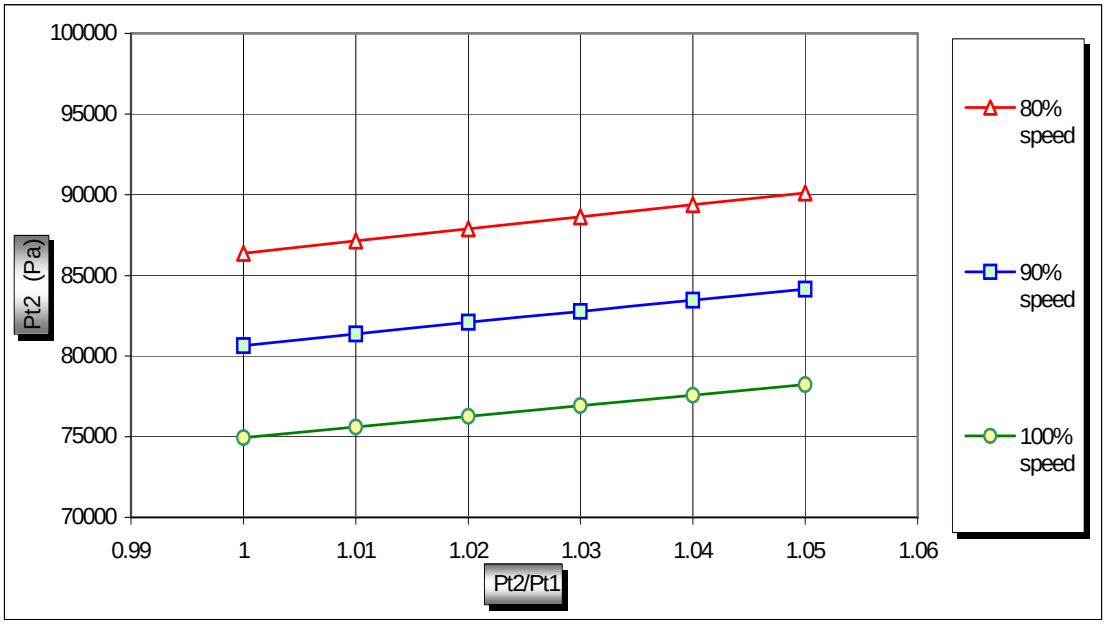

Figure 8. Injection stagnation pressure variation with distortion parameter π (α =0.08, $\nu = 1.05$)

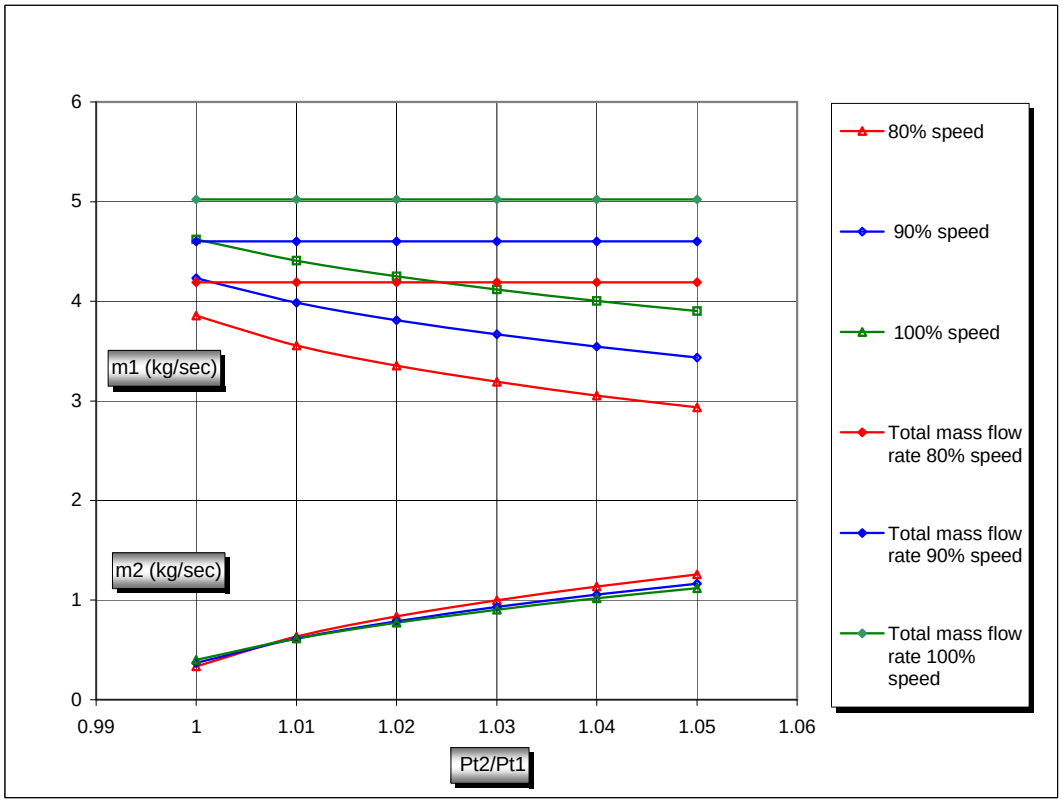

Figure 9. Mass flow-rate variation with distortion parameter (α =0.08, ν=1.05)

Figure 7 shows that when π increases, M_2 rises at a much higher rate than the rate at which M_1 decreases. Similarly, in Figure 9 m_2 increases and m_1 decreases with increasing distortion. The required stagnation pressure in the injected flow Pt_2, increases with π but remains lower than standard atmospheric pressure (101325 Pa). Therefore, the injected flow can be fed from the atmosphere and the pressure controlled using a throttle. With the throttle in the injected flow, the amplitude of Pt_2 can be adjusted, while the throttle in the main flow can be used to adjust the overall level of Pt_3.

C. TEMPERATURE DISTORTION GENERATION

1. Analysis

The following assumptions were made:

1. Neglect effect of friction at the wall
2. The two flows are at the same stagnation pressure ($\pi = 1$)
3. After mixing, the flow is uniform at station 3.
4. The flow from station 3 to station 4 is isentropic ($Pt_3 = Pt_4$, $Tt_3 = Tt_4$)
5. The injected stream enters parallel to the main stream, so that $P_1 = P_2$.

With these assumptions, the equations for conservation of mass, momentum and energy remain the same as given for the analysis of pressure distortion in Equations 1, 2 and 3 respectively. Also, as before, the area fraction α in Equation 4 must be selected to have a value $0<\alpha<1$. Furthermore, it is again assumed that Pt_3 is a fraction of Pt_{3d} ($\frac{Pt_3}{Pt_{3d}} = \nu > 1$) to account for an expected degradation in pumping capability with inlet distortion. Finally, since the main flow will always be pumped from the atmosphere, it will be assumed that $Tt_1 = Tt_{3d}$.

The magnitude of the temperature distortion is defined by the value of $\tau = \frac{Tt_2}{Tt_1}$.

While both $\tau > 1$ and $\tau < 1$ are of interest, $\tau > 1$ can be implemented more easily, using a heater in the auxiliary flow. Since the stagnation pressures are the same, and the static pressure is common, the Mach number in the main flow is the same as in the injected flow. Thus $M_1 = M_2$, $T_2 = T_1\tau$, and the entering velocities are different.

The analytical approach followed was again to eventually express all the quantities in terms of the unknown Mach number at station 1, M_1. The development is described in a series of steps.

1. Assume a Pt_3 smaller or bigger than Pt_{3d}. The value of Pt_{3d} is taken from experimental data presented in Appendix A for 90% operational level of speed.

$$\frac{Pt_3}{Pt_{3d}} = \nu \ <1 \text{ or } >1 \tag{13}$$

Note that the corrected flow rate is then known from the compressor map.

2. Using Equation 9 at stations 1 and 2, with $\pi = 1$, $M_1 = M_2$ and τ given, and writing $\lambda = \frac{(1-\alpha)}{\alpha}$,

$$m_1 = (\lambda\sqrt{\tau})m_2 \tag{14}$$

and using Equation 1,

$$m_1 = \left(\frac{\lambda\sqrt{\tau}}{\lambda\sqrt{\tau}+1}\right)m_3 \tag{15}$$

3. Using Equations 14 and 15 in Equation 2,

$$Tt_3 = \left(\frac{\tau+\lambda\sqrt{\tau}}{1+\lambda\sqrt{\tau}}\right)Tt_1 \tag{16}$$

Since Tt_3 is now known, using the corrected flow rate and Pt_3, the flow rate m_3 is obtained; then m_1 and m_2 are given by Equations 15 and 16, respectively.

4. Using Equation 9 (at stations 1 and 2) in Equation 3,

$$0 = \left(\frac{m_1 M_1 (\gamma R T t_1)^{0.5} + m_2 M_1 (\gamma R \tau T t_1)^{0.5}}{\left(1+\left(\frac{\gamma-1}{2}\right)M_1^{\,2}\right)^{0.5}}\right) - m_3 V_3 + A_3\left[\frac{m_1 \frac{(RTt_1)^{0.5}}{A_1\gamma^{0.5}}}{M_1\left(1+\left(\frac{\gamma-1}{2}\right)M_1^{\,2}\right)^{(h+b)}} - P_3\right] \tag{17}$$

where the exponents are $h = \frac{-(\gamma+1)}{2(\gamma-1)}$ and $b = \frac{\gamma}{\gamma-1}$.

Since V_3 and P_3 in Equation 17 can be written in terms of stagnation pressure and temperature, which are known, and Mach number, which is obtained from Equation 9, the only unknown is M_1.

An EES code was written to evaluate first M_1 and then calculate all the other unknowns (Appendix D).

2. Results

The inlet temperature distortion design calculations were again based on the assumption that $\frac{Pt_3}{Pt_{3d}} = \nu = 1.05$ (that the compressor pumping capability would deteriorate with distortion present), and that the corrected flow rate, $m_c = \frac{m\sqrt{T_t / T_{std}}}{P_t / P_{std}}$, would be given by the experimentally determined compressor map shown in Figure 3. From preliminary calculations of the power required for different areas of the injected flow, a value of α=0.08 was selected. Results were then obtained for temperature distortion values of τ from 1.05 to 1.25.The results are given in Figures 10-12 for operation (near stall) at 80%, 90% and 100% of design speed.

The Mach number in the main and secondary streams is shown in Figure 10. The amount of energy transferred to the injected flow at stations 1 and 2, required to satisfy Pt_3=1.05 Pt_{3d}, is shown in Figure 11, and the mass flow rates of the two streams are shown in Figure 12. Note that all the blue colored curves are for the minimum design corrected mass flow rate at 90% operational speed.

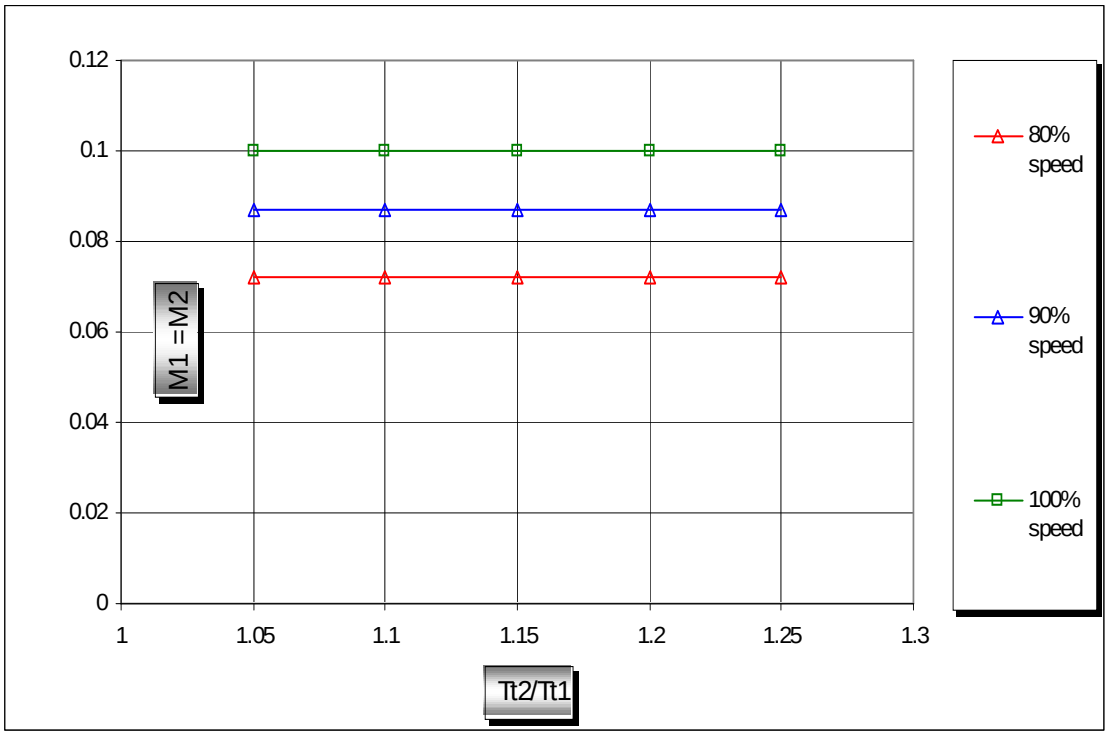

Figure 10. Mach number variation with temperature distortion parameter τ (α=0.08, ν=1.05)

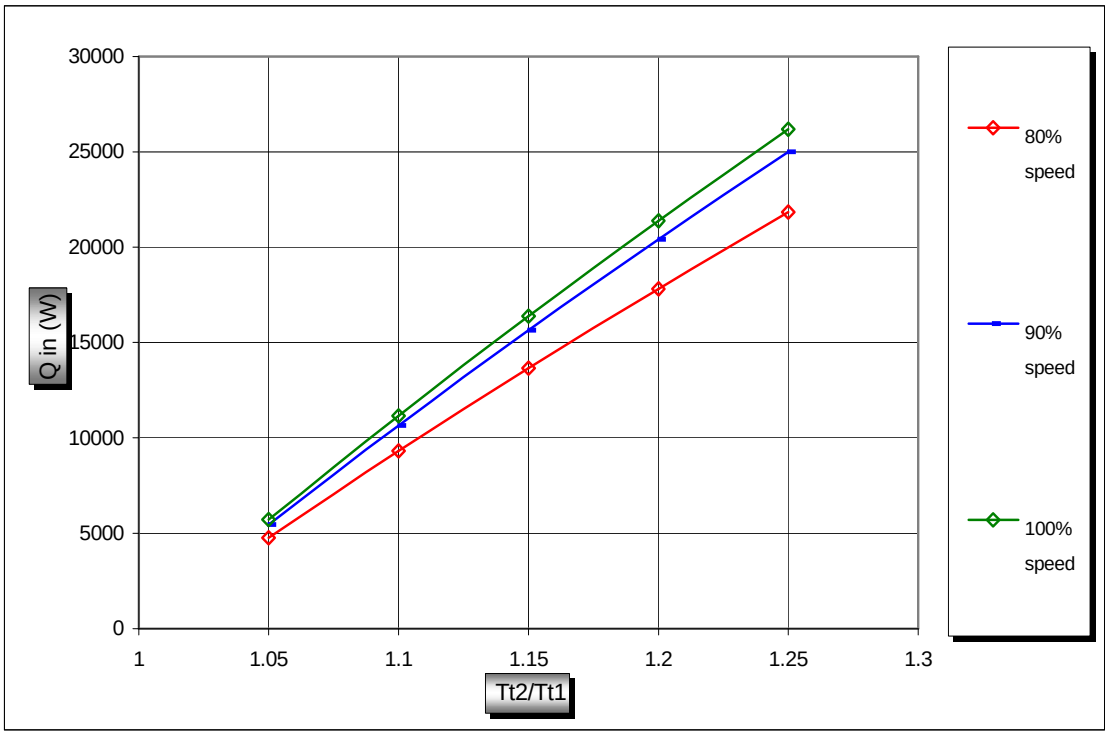

Figure 11. Energy required to heat the injected flow (α=0.08, ν=1.05)

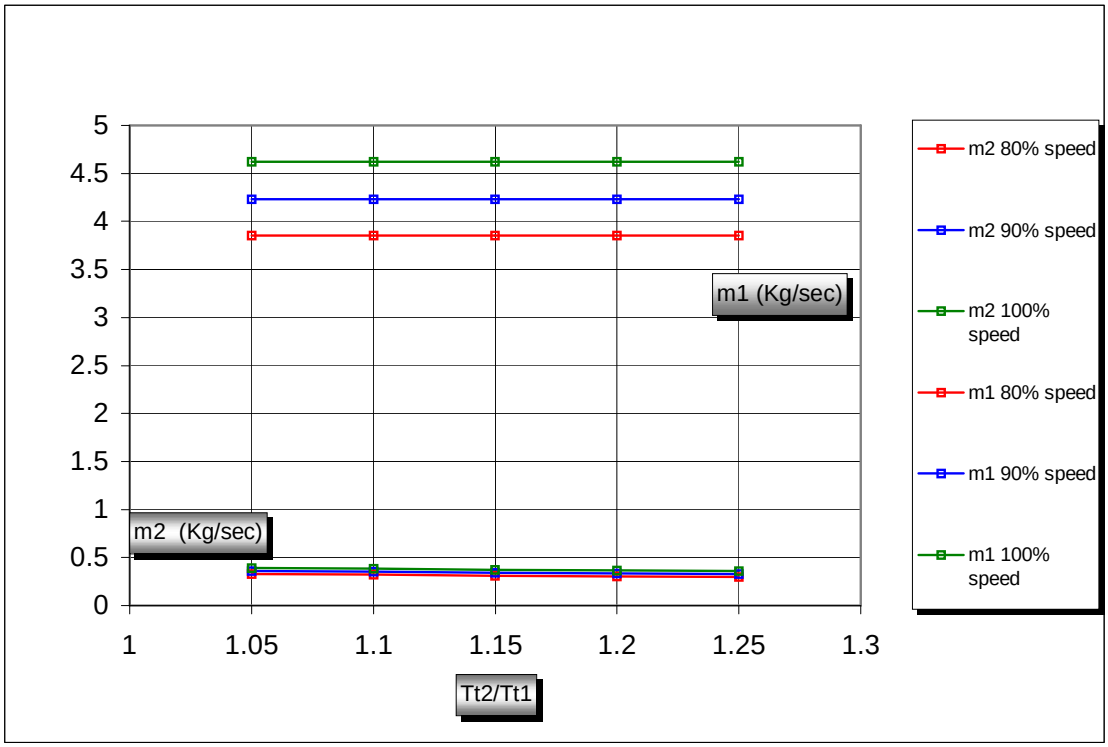

Figure 12. Mass flow-rate variation with distortion parameter τ (α =0.08, ν=1.05)

Figure 10 shows that when the magnitude of τ increases, M_1 (and therefore M_2) remains approximately constant. Similarly, as τ increases, there is little effect on the mass flow rates in the two streams. This is to be expected since it has been assumed that the stagnation temperature in the main flow will not change. The energy required to heat the injected flow is seen to increase directly with τ. The data in Figure 11 explains the particular selection made for the injection duct area ratio. With the selection of α=0.08, it was possible to vary τ up to 1.25 without exceeding 25 kW in the required power.

THIS PAGE INTENTIONALLY LEFT BLANK

IV. COMPUTATIONAL ANALYSIS OF DISTORTION GENERATION

In the previous chapter the analysis of the auxiliary injection assumed that uniform ("fully mixed out flow") conditions occurred at the downstream station, and this allowed the downstream boundary condition to be related to the compressor-pumping characteristic (or "map") at Station 4. The analysis properly conserved mass, momentum and energy, and served to allow the size of the auxiliary duct exit to be selected as shown in Figure 13. In reality, the auxiliary and main flows will not be fully mixed out, and the flow at the compressor face will depend on the position of the auxiliary duct exit forward of the compressor; i.e. on the selection of the "mixing length", L, shown in Figure 14.

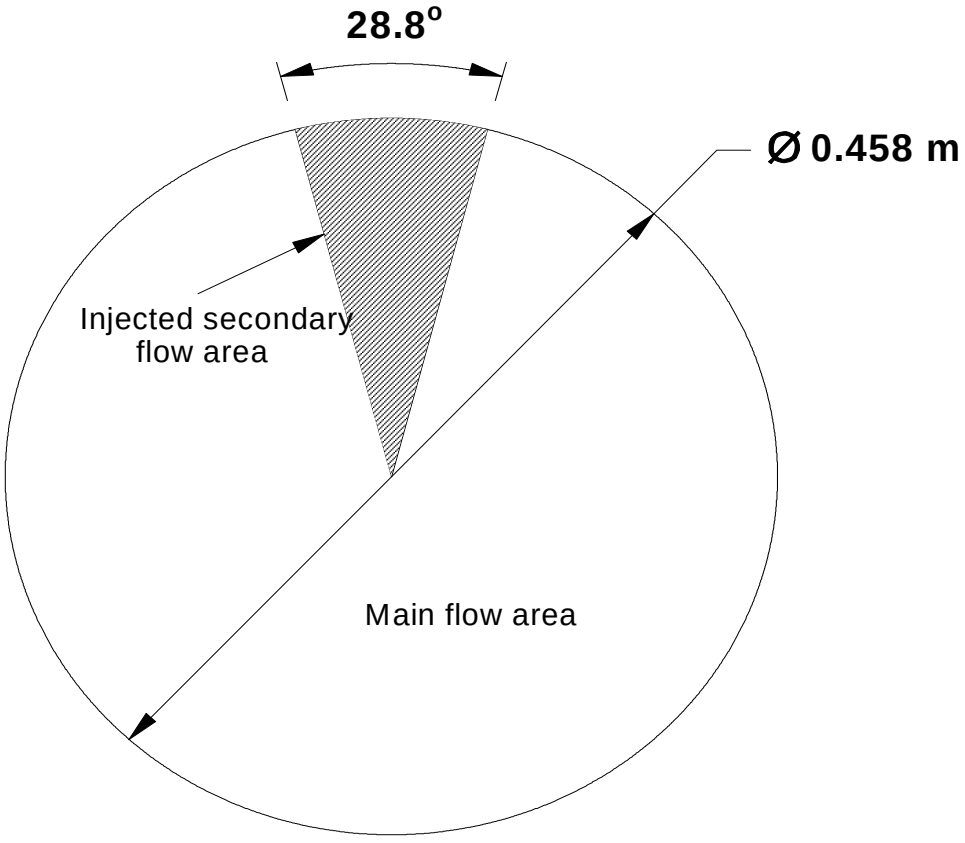

Figure 13. Injected flow area

A computational analysis of the compressible mixing was carried out using the CFD code ACE (References 8, 9, and 10). Figure 14 shows the geometry that was modeled in order to evaluate the mixing for 3 different locations of the exit of the auxiliary duct; specifically, for L=0.5, 1.0 and 2.0 meters.

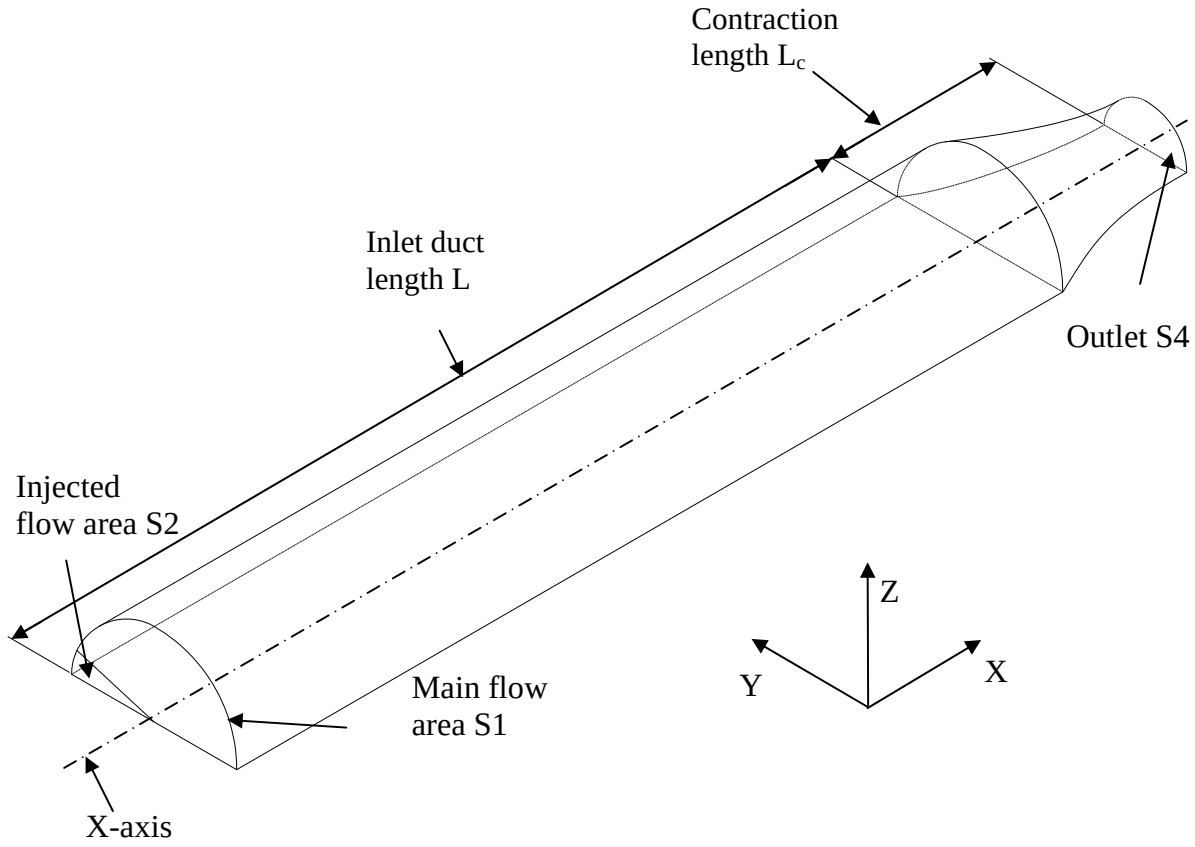

Figure 14. Geometry of the duct used in CFD ACE code.

ACE is one of a set of computer codes for multi-physics computational analysis developed by CFDRC. The codes provide an integrated geometry and grid generation module, CFD-GEOM; a graphical user interface for preparation of the model, a computational solver for performing the simulation, CFD-ACE (U), and an interactive visualization program for examination and analysis of the simulation results, CFD-VIEW.

There are provisions to create a computational grid with boundaries that can be classified as symmetry, inlet, outlet, wall or 'arbitrary'. Stagnation pressure and temperature can be specified and held at the inlet, static pressure can be specified and held at the outlet. In order to compute the flow corresponding to π = 1.05 (pressure distortion) or τ = 1.25 (temperature distortion), the inlet stagnation pressure level was adjusted until the mass flow rate was equal to the required value.

An example of the computational grid generated to model the main duct with an auxiliary inlet duct occupying 8% of the annulus is shown in Figure 15. Note that a rectangular region was required along the axis to avoid the singularity from a center axis.

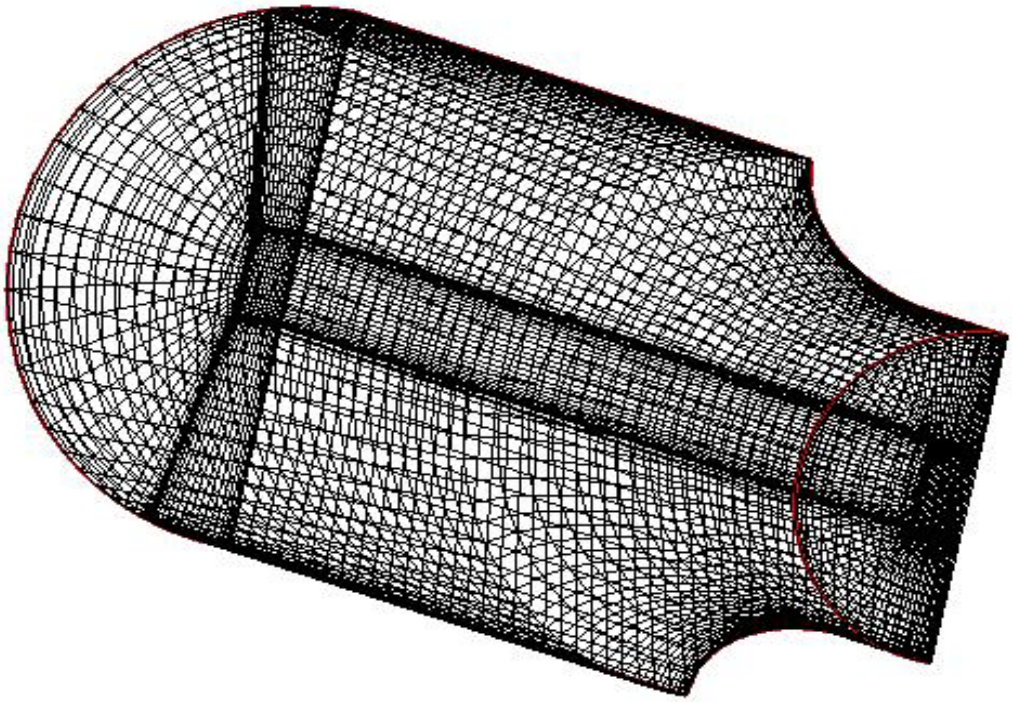

Figure 15. Example of the grid used to calculate the mixing from auxiliary injection

When the grid was satisfactory, a converged solution (three orders of magnitude reduction of residuals) could be obtained, as shown in Figure 16 for one case of pressure distortion. Figure 16 shows the larger inlet pipe, with uniform inflow over the auxiliary injection sector, and the mixed profile at the exit (compressor face) after the area contraction. In order to compare the profiles generated with different mixing lengths, data

at the outlet boundary were plotted along the two lines shown in Figure 16 and dimensioned in Figure 17. Results obtained for pressure and temperature distortion are described in the following sections.

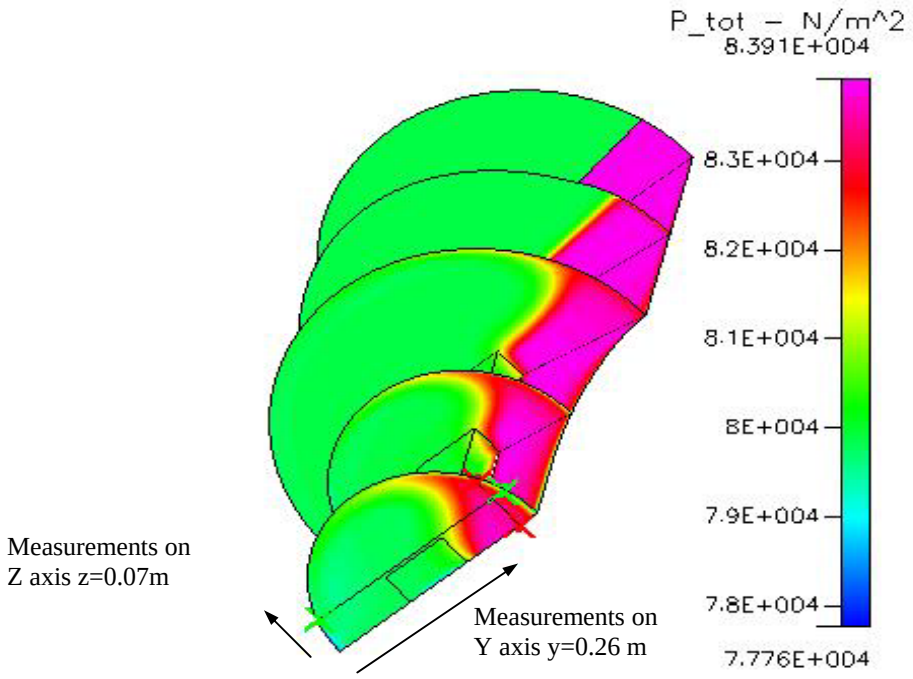

Figure 16. Inlet to exit flow and lines chosen at the exit for data comparison

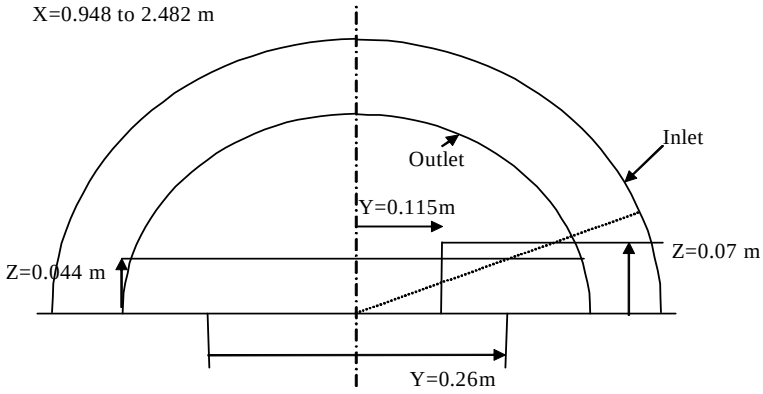

Figure 17. Locations that were selected at the exit plane (station 4) to compare results

A. PRESSURE DISTORTION

The results of calculating the mixing with the auxiliary flow injected at 5% higher in stagnation pressure (π = 1.05), but at the same stagnation temperature (τ =1), as the main flow, for three different mixing lengths, are shown in Figures 18 and 19.

Figure 16 and 17 shows the locations that were selected at the exit plane (station 4) to compare results. It is observed that the levels of inlet stagnation pressures were higher than these that were used in corresponding cases in chapter III, since the exit static pressure and flow rate were the same but the exit was not fully mixed out.

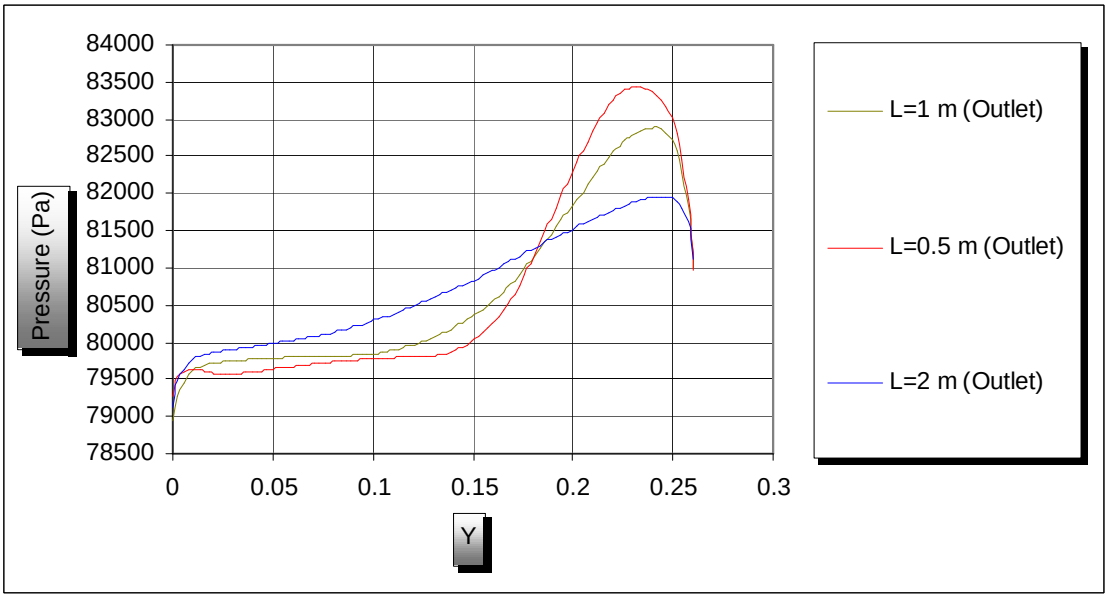

Figure 18. Stagnation pressure distribution at station 4 (at Z = 0.044 m) for different inlet duct lengths (90% speed, π = 1.05, τ = 1)

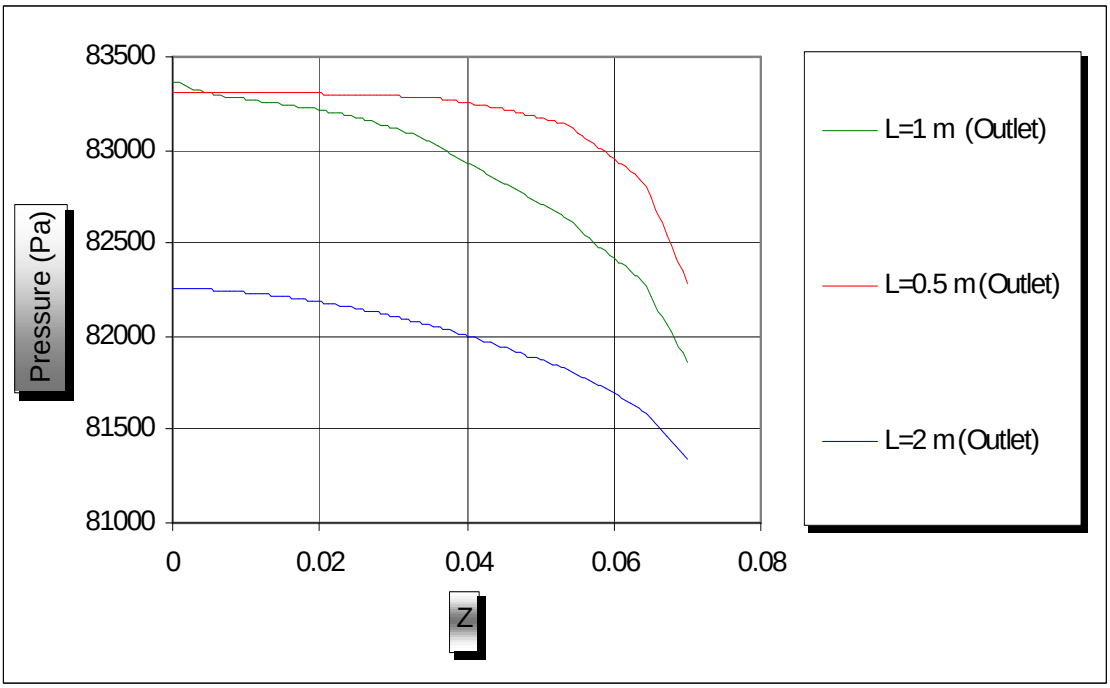

Figure 19. Stagnation pressure distribution at station 4 (at Y = 0.115 m) for different inlet duct lengths (90% speed, π = 1.05, τ = 1)

B. TEMPERATURE DISTORTION

The results of calculating the mixing with the auxiliary flow injected at 25% higher stagnation temperature (τ = 1.25), but at the same stagnation pressure (π = 1.0) as the main flow, for three different mixing lengths, are shown in Figures 19 and 20. Figure 16 shows the locations that were selected at the exit plane (station 4) to compare results. Again it is observed that the levels of inlet stagnation pressures were higher than those that were used in corresponding cases in chapter III, since the exit static pressure and flow rate were the same but the exit was not fully mixed out.

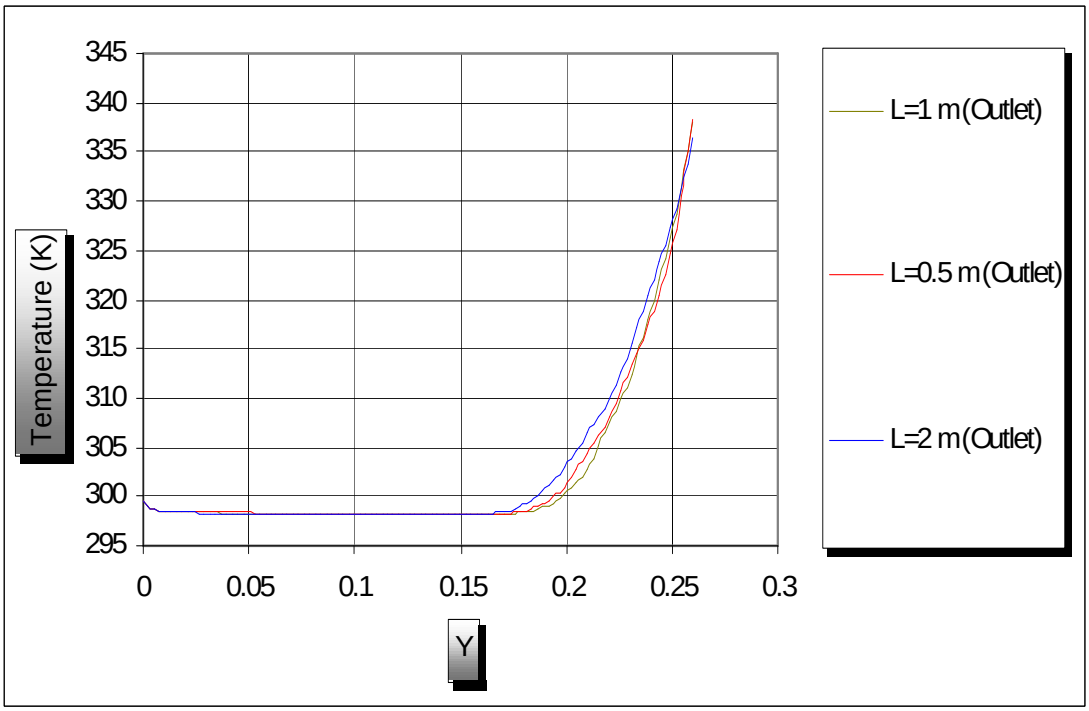

Figure 20. Stagnation temperature distribution at station 4 (at Z = 0.044 m) for different inlet duct lengths (90% speed, π = 1.0, τ = 1.25)

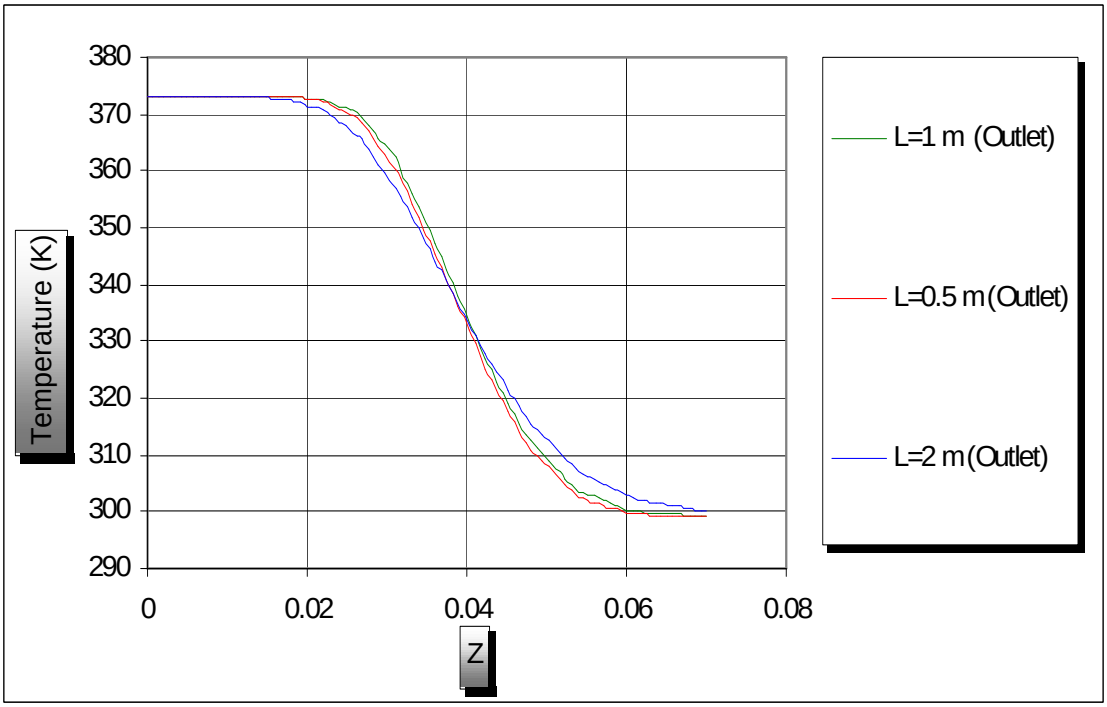

Figure 21. Stagnation temperature distribution at station 4 (at Y = 0.115 m) for different inlet duct lengths (90% speed, π = 1.0, τ = 1.25)

From Figures 18-21, it can be seen that the mixing in the case of temperature distortion is less than for pressure distortion, although the magnitude of the distortion parameter is larger (τ = 1.25 compared to π = 1.05). In fact, what drives the mixing is the difference in the incoming velocities of the two streams. It can be shown (Appendix E) that $\frac{V_2}{V_1} = \sqrt{\tau}$ when π = 1.0, but that $\frac{V_2}{V_1} = \sqrt{\frac{2}{(\gamma-1)M_1^2}\left[1-\pi^{-\left(\frac{\gamma-1}{\gamma}\right)}\right]+1}$ when τ = 1.0. Since the Mach number in the inlet pipe is low (~ 0.07), $\frac{V_2}{V_1} = 3.85$ for the pressure distortion case analyzed (π = 1.05) compared to 1.12 for the temperature distortion case analyzed (τ = 1.25). These values of relative inlet velocity were confirmed by the code.

C. GRID SENSITIVITY

The sensitivity of the CFD code predictions to different grid selections was evaluated for the 0.5 meter mixing length geometry. Three different grids were used, progressively increasing the number of nodes. Grid 1 had 37,908 nodes, Grid 2 had 85,183 nodes and Grid 3 had 128,478 nodes. The results are shown in Figures 22-25. It can be seen (in Figure 23) that the largest effect of the grid selection was from Grid 1 to Grid 2 in the case of pressure distortion. However, from Grid 2 to Grid 3 there were very small differences in the results for both pressure and temperature distortion. Consequently, Grid 2 was used for the 0.5 meter mixing length, and a similar grid density was used when extending the inlet duct length (100,103 nodes for the one meter and 133,366 nodes for the two meter length).

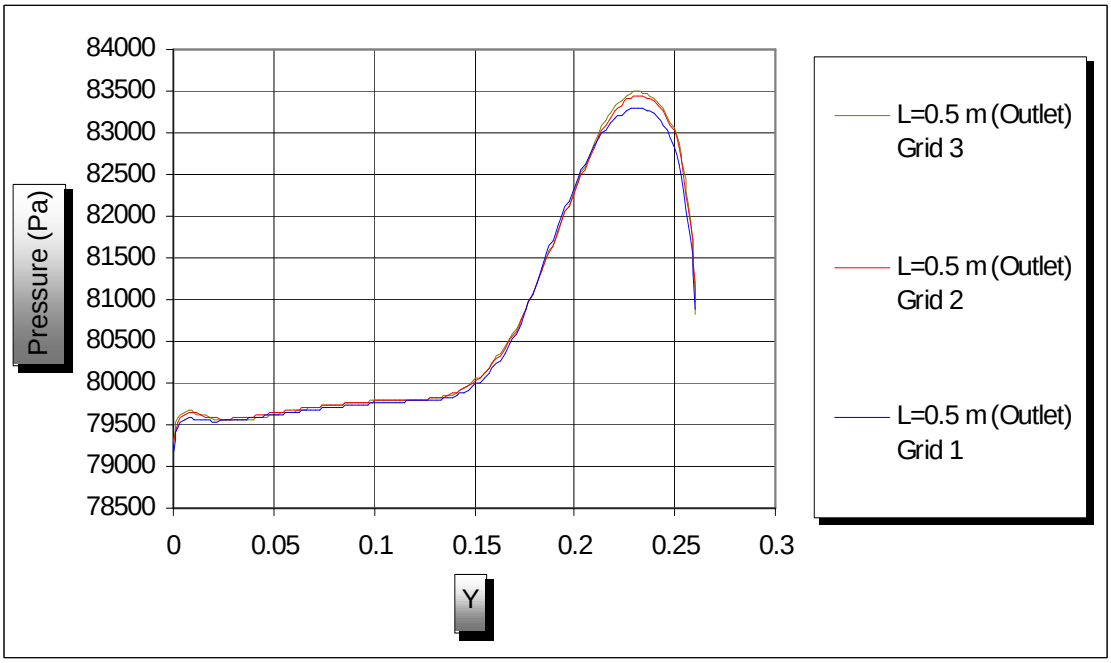

Figure 22. Stagnation pressure distribution at station 4 (at Z = 0.044 m) for different grid selection (90% speed, π = 1.05, τ = 1)

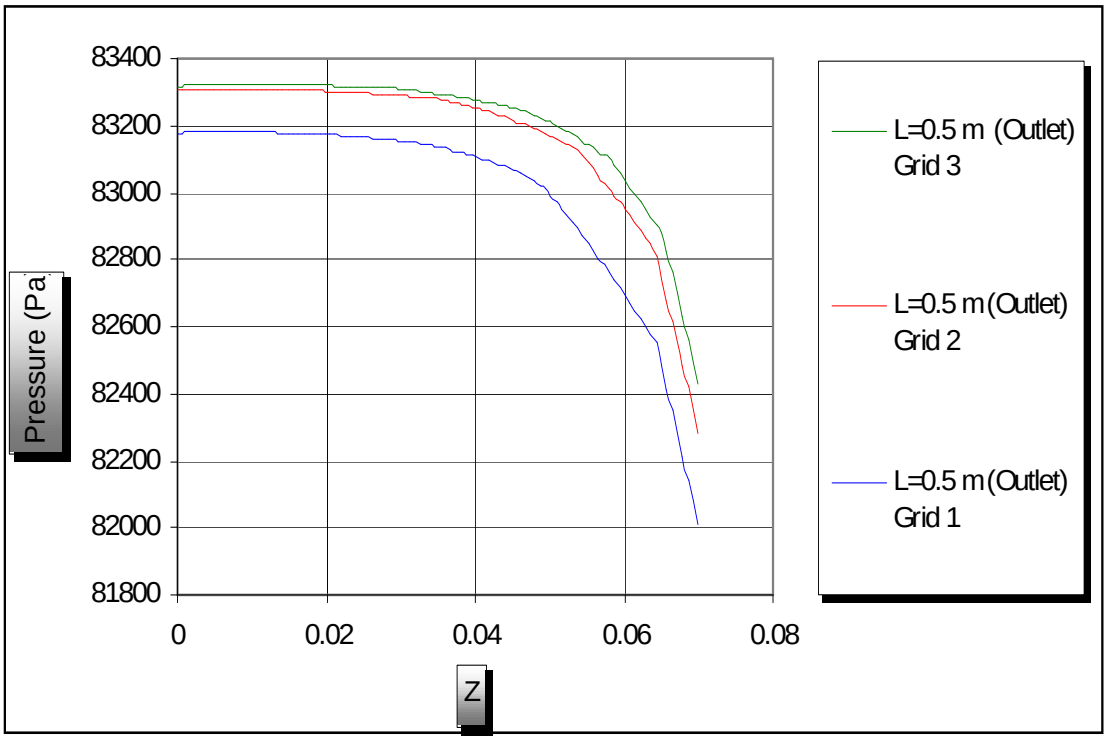

Figure 23. Stagnation pressure distribution at station 4 (at Y = 0.115 m) for different grid selection (90% speed, π = 1.05, τ = 1)

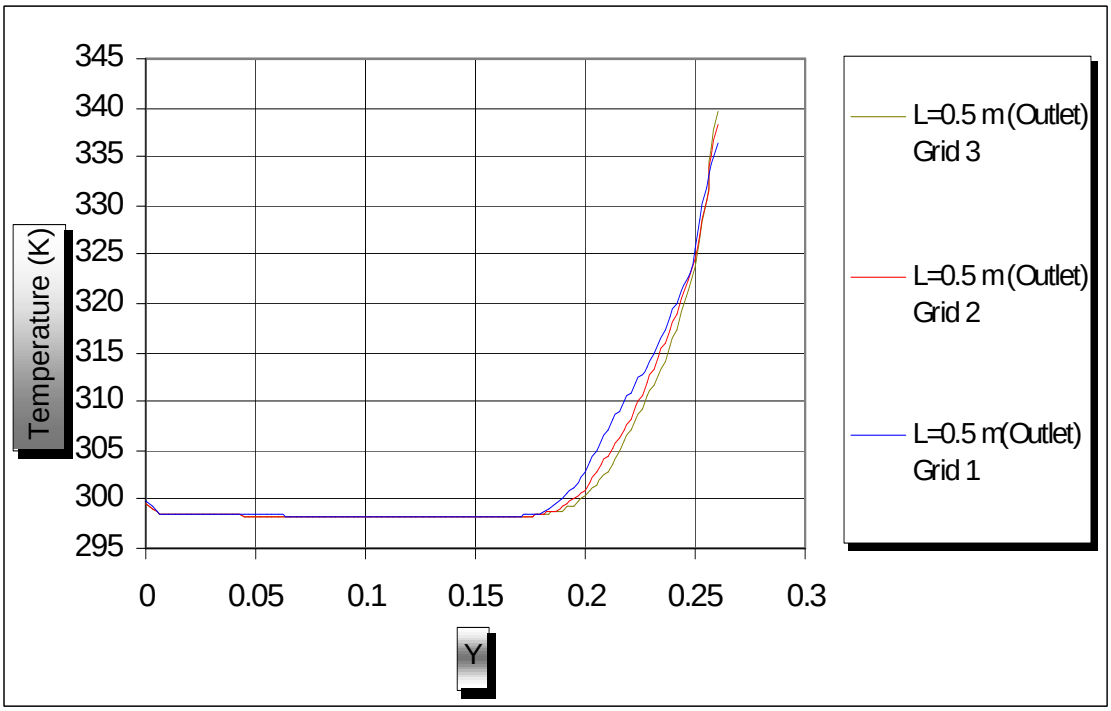

Figure 24. Stagnation temperature distribution at station 4 (at Y = 0.115 m) for different grid selection (90% speed, π = 1.0, τ = 1.25)

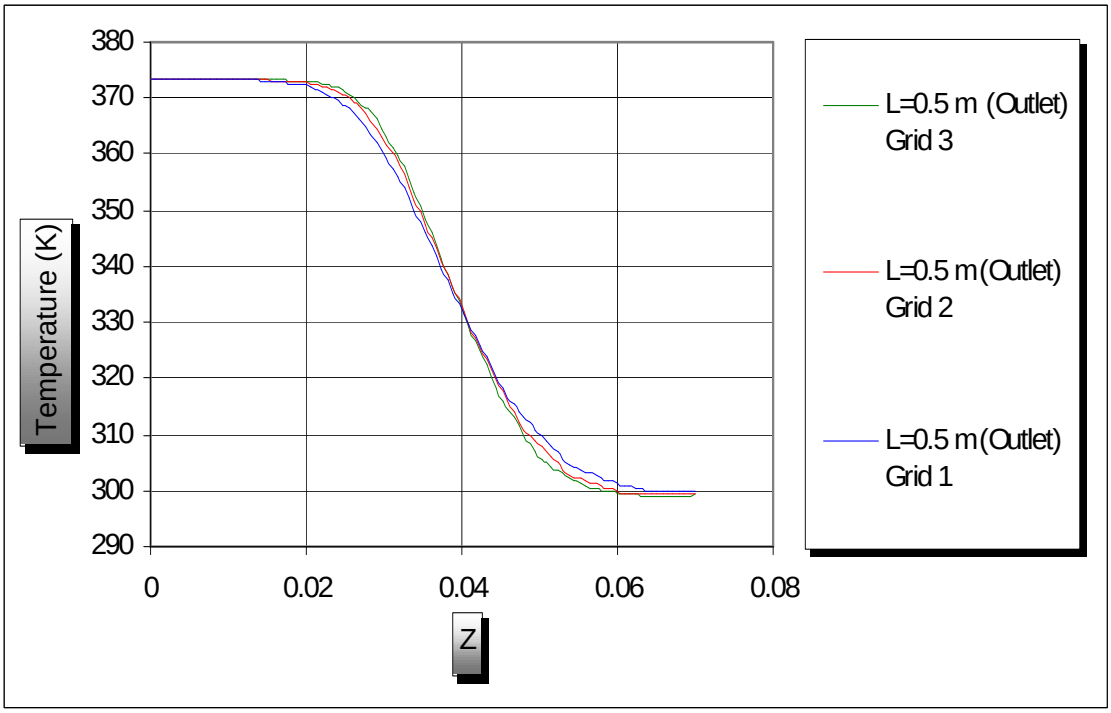

Figure 25. Stagnation temperature distribution at station 4 (at Z = 0.044 m) for different grid selection (90% speed, π = 1.0, τ = 1.25)

V. CONCLUSIONS AND RECOMMENDATIONS

The present study was motivated by the need to conduct controlled experiments on the effect of steam or hot-air ingestion on the stability and stall margin of gas-turbine engine compressors. The proposal to use auxiliary injection into the inlet pipe of the NPS transonic compressor was examined. The following were concluded:

- It is feasible to generate and control pressure and temperature distortion using air ingestion through an auxiliary duct incorporating one additional auxiliary throttle valve.
- Using a 25 KW heater, a suitable range of temperature distortion can be developed using an auxiliary duct area equal to 8% of the inlet pipe.
- Two engineering codes (EES) were generated to calculate inlet conditions from the compressor characteristic for specified pressure and temperature distortion parameters. The code calculations enabled the auxiliary duct size to be selected.
- A CFD analysis was carried out successfully to determine the flow profile entering the compressor and the effect of the available mixing length. The results were shown to be insensitive to grid selection.

The following recommendations are made:

- Extend the CFD simulation to include the full geometry of the injection duct
- Complete the inlet hardware design (with provision to position the auxiliary duct at different locations)
- Design, or select, a suitable air heater
- Procure a steam generator to inject through the same duct.
- Make provision for the measurement of secondary air/steam mass flow rate, pressure and temperature.

THIS PAGE INTENTIONALLY LEFT BLANK

APPENDIX A TEST AND INLET DISTORTION DATA

A. EXPERIMENTAL PERFORMANCE MAP

Table 1. 80% operational speed data

Run no							
1	Mass Flow	Pt_ratio	Tt4d(0c)	Pt4d	P4d	RPM	M4
2	3.99164818	1.344786	16.8304362	82257.85	79766.09	21827.19	0.210088
3	4.19552573	1.337583	17.69664714	83233.64	80499.93	21799.52	0.218943
4	4.583530331	1.322167	17.61668294	85164.86	82133.92	21791.87	0.228117
5	4.945168818	1.318621	17.71622721	86862.63	83228.69	21786.58	0.247841
6	5.203798788	1.309887	17.02320964	88343.52	84513.06	21755.76	0.252441
7	5.814255239	1.27468	17.80014648	93667.14	89144.06	21794.26	0.266848
8	6.055224276	1.258274	17.17148438	96307.87	91439.04	21793.18	0.273245
9	6.178094964	1.252228	17.30166016	97353.23	92371.1	21769.75	0.274975

Table 2. 90% operational speed data

Run no							
1	Mass Flow	Pt_Ratio	Tt4d(0c)	Pt4d	P4d	RPM	M4
2	4.381216587	1.46121522	29.4043457	76802.92	73402.47	25086.49	0.255173
3	4.468290403	1.45931496	14.98787435	76679.29	73529.92	24394.9	0.245507
4	4.512427704	1.45328577	15.70483398	77083.1	73692.37	24380.09	0.25432
5	4.839665367	1.4535476	29.01258138	77784.41	74220.32	24922.73	0.259721
6	5.080933861	1.43758367	16.29047309	79539.32	75537.24	24434.66	0.272576
7	5.345904496	1.4294289	28.50551758	81149.71	76826.74	24974.81	0.280747
8	5.661951478	1.41257914	14.23828125	83281.68	78574.72	24362.89	0.289494
9	5.681440546	1.40218943	28.14306641	85147.89	79734.49	25014.69	0.307775
10	6.034647541	1.37024027	29.19163411	88890.65	83267.79	24946.83	0.306964
11	6.036431418	1.38713393	27.87753906	87052.26	81500.33	24916.78	0.308281
12	6.220627881	1.37083823	15.25431315	88720.71	83176.34	24373.44	0.305027
13	6.697960407	1.32553477	29.42128906	95424.21	89074.93	25078.21	0.315178
14	6.873528918	1.32203335	14.99145508	95457.43	89226.49	24323.46	0.312039

Table 3. 100% operational speed data

Run no							
1	Mass Flow	Pt_Ratio	Tt4d(0c)	Pt4d	P4d	RPM	M4
2	4.783778964	1.593625	17.10299479	71356.82	67204.76	27146.95	0.293903
3	4.878505613	1.574358	20.42115885	72519.86	68110.02	27072.63	0.300718
4	4.964007749	1.57407	17.38203125	73093.4	68717.47	26899.6	0.298286
5	5.276035803	1.571927	15.20699685	74177.01	69238.64	26940.92	0.315272
6	5.293451804	1.55561	18.13105469	74840.54	70316.04	26803.71	0.299806
7	5.378261808	1.554052	21.20722656	74850.87	68825.11	27103.79	0.34835
8	5.417627178	1.561808	16.52239583	74722.02	69676.13	27065.13	0.317625
9	5.629933906	1.547752	18.37011719	76626.1	71312.47	27067.99	0.322068
10	6.060280342	1.509242	19.17338867	80292.57	74308.21	26936.42	0.334491
11	6.076155446	1.517941	15.41518555	79847.25	73591.53	26972	0.343395
12	6.346813703	1.479708	20.77011719	82624.98	76112.9	26978.9	0.344476
13	6.370598575	1.476179	17.33754883	83590.99	76989.97	27028.21	0.344829
14	6.48758399	1.481319	18.94223633	83939.83	77282.39	27102.85	0.34562
15	6.487651075	1.48281	15.18090123	83668.5	76948.11	26965.11	0.347934
16	6.749165973	1.455565	15.13730469	86549.18	79670.71	26983.19	0.345994
17	7.06954336	1.415859	18.0215332	90534.76	83122.17	27132.38	0.351473
18	7.262751202	1.388472	21.27998047	93822.34	86224.78	27121.16	0.349433
19	7.278570267	1.399183	18.88925781	93361.07	85801.28	27002.95	0.349423
20	7.400624968	1.389324	18.53776042	94515.02	86937.39	26934.37	0.347596
21	7.458758542	1.393771	15.44352214	94426.45	86798.42	27020.12	0.348987

B. PRESSURE DISTORTION

In the following tables small changes to the used so far symbols are made, and are presented from the notation below.

Notation:

a Ratio of secondary to overall flow area ($a = \frac{A2}{A3}$)

p Ratio of secondary to main-flow stagnation pressure ($p = \frac{Pt2}{Pt1}$)

mt Total mass flow rate mt=m1+m2

Table 4. Mass flow vs. pressure ratio p

p	a	m1(80)	m1(90)	m1(100)	m2(80)	m2(90)	m2(100)	mt(80)	mt(90)	mt(100)
1	0.08	3.856	4.232	4.621	0.3353	0.368	0.4018	4.1913	4.6	5.0228
1.01	0.08	3.556	3.986	4.409	0.635	0.6138	0.6143	4.191	4.5998	5.0233
1.02	0.08	3.355	3.812	4.251	0.8358	0.7885	0.7722	4.1908	4.6005	5.0232
1.03	0.08	3.194	3.669	4.12	0.9973	0.9313	0.9033	4.1913	4.6003	5.0233
1.04	0.08	3.055	3.545	4.005	1.136	1.055	1.018	4.191	4.6	5.023
1.05	0.08	2.933	3.435	3.903	1.259	1.165	1.12	4.192	4.6	5.023

Table 5. Mach number vs pressure ratio p

p	a	M1(80)	M1(90)	M1(100)	M2(80)	M2(90)	M2(100)
1	0.08	0.07226	0.08688	0.1002	0.07226	0.08688	0.1002
1.01	0.08	0.06668	0.08188	0.09559	0.1367	0.1448	0.153
1.02	0.08	0.06297	0.07836	0.09224	0.1799	0.1859	0.1922
1.03	0.08	0.06001	0.0755	0.08948	0.2146	0.2194	0.2247
1.04	0.08	0.05747	0.07303	0.08708	0.2443	0.2485	0.253
1.05	0.08	0.05523	0.07084	0.08494	0.2707	0.2744	0.2784

Table 6. Injected flow stagnation pressure vs. pressure ratio p

p	a	P80	P90	P100
1	0.08	86371	80643	74925
1.01	0.08	87143	81368	75601
1.02	0.08	87897	82077	76263
1.03	0.08	88642	82778	76918
1.04	0.08	89383	83473	77567
1.05	0.08	90120	84165	78213

C. TEMPERATURE DISTORTION

Table 7. Mass flow vs. temperature ratio t

t	a	m1(80)	m1(90)	m1(100)	m2(80)	m2(90)	m2(100)	mt(80)	mt90)	mt(100)
1.05	0.08	3.856	4.232	4.621	0.3272	0.3591	0.3921	5.734	6.396	6.839
1.1	0.08	3.856	4.232	4.621	0.3197	0.3509	0.3831	5.723	6.384	6.826
1.15	0.08	3.855	4.231	4.62	0.3126	0.3431	0.3746	5.713	6.373	6.814
1.2	0.08	3.855	4.231	4.62	0.306	0.3359	0.3667	5.704	6.362	6.802
1.25	0.08	3.854	4.23	4.619	0.2998	0.329	0.3592	5.694	6.351	6.791

Table 8. Mach number vs. temperature ratio t

t	a	M1(80)	M1(90)	M1(100)	M2(80)	M2(90)	M2(100)
1.05	0.08	0.07225	0.08688	0.1002	0.07225	0.08688	0.1002
1.1	0.08	0.07225	0.08688	0.1001	0.07225	0.08688	0.1001
1.15	0.08	0.07224	0.08687	0.1001	0.07224	0.08687	0.1001
1.2	0.08	0.07223	0.08686	0.1001	0.07223	0.08686	0.1001
1.25	0.08	0.07222	0.08684	0.1001	0.07222	0.08684	0.1001

Table 9. Heat transfer to the injected flow vs. temperature ratio t

t	a	Q80	Q90	Q100
1.05	0.08	4766	5457	5717
1.1	0.08	9311	10663	11170
1.15	0.08	13659	15642	16385
1.2	0.08	17826	20414	21384
1.25	0.08	21829	24998	26186

APPENDIX B MASS FLOW RATE EQUATION

The (uniform) mass flow rate at any section with area A is given by

$$m = \rho \mathrm{A} V \tag{1}$$

Substituting for the density using the equation of state,

$$\rho = \frac{P}{RT} \tag{2}$$

and for the velocity using the definition of Mach number,

$$V = M\sqrt{\gamma RT} \tag{3}$$

and then introducing the relationships between static and stagnation properties,

$$P = Pt\left(1 + \frac{(\gamma - 1)}{2} M^2\right)^{-\frac{\gamma}{(\gamma-1)}} \tag{4}$$

and

$$T = Tt\left(1 + \frac{(\gamma - 1)}{2} M^2\right)^{-1} \tag{5}$$

Equation 1 can be written as

$$m = \frac{Pt\mathrm{A}}{\sqrt{\gamma RTt}} \gamma M\left(1 + \frac{(\gamma - 1)}{2} M^2\right)^{-\frac{(\gamma+1)}{2(\gamma-1)}} \tag{6}$$

THIS PAGE INTENTIONALLY LEFT BLANK

APPENDIX C PRESSURE DISTORTION (EES CODE)

In the EES codes listed in Appendices C and D some changes were made to the notation used previously. The following lists departures from the previous notation:

Notation:

u	Velocity
k	Ratio of specific heats (here, k=1.4)
a	Ratio of secondary to overall flow area ($a = \frac{A2}{A3}$)
p	Ratio of secondary to main-flow stagnation pressure ($p = \frac{Pt2}{Pt1}$)
t	Ratio of secondary to main-flow stagnation temperature ($t = \frac{Tt2}{Tt1}$)
n, p2	Ratio of stagnation pressure at station 3 to design value ($n = p2 = \frac{Pt3}{Pt3d}$)

$$m4d = 4.381$$

$$Pt4d = 76803$$

$$D4 = \frac{11}{12 \cdot 3.28}$$

$$A4 = \pi \cdot \frac{D4^{2}}{4}$$

$$K = 1.4$$

$$R = 287$$

$$cp = R \cdot \left[\frac{K}{K - 1}\right]$$

$$TT = 29.4$$

$$Tt4d = TT + 273.15$$

$$D3 = \frac{18}{12 \cdot 3.28}$$

$$A3 = \frac{D3^{2}}{4} \cdot \pi$$

$$a = 0.08$$

$$A2 = a \cdot A3$$

$$A2 = A1 \cdot \left[\frac{a}{1 - a}\right]$$

$$Tt1 = Tt4d$$

$$Tt2 = Tt1$$

$$Tt3 = \left[\frac{1}{a \cdot \left(\frac{p}{1 - a}\right) + 1} + \frac{1}{1 + \frac{1 - a}{a \cdot p}}\right] \cdot Tt1$$

$$Pt2 = p \cdot Pt1$$

$$p = \text{Pressureratio}$$

$$h = \frac{-(K + 1)}{2 \cdot (K - 1)}$$

$$m4d = Pt4d \cdot \frac{A4}{Tt4d^{0.5}} \cdot \left[\frac{K}{R}\right]^{0.5} \cdot Ma4d \cdot \left[1 + \left(\frac{K - 1}{2}\right) \cdot Ma4d^{2}\right]^{h}$$

$$Pt3d = Pt4d$$

$$Tt3d = Tt4d$$

$$m3d = m4d$$

$$m3d = Pt3d \cdot \frac{A3}{Tt3d^{0.5}} \cdot \left[\frac{K}{R}\right]^{0.5} \cdot Ma3d \cdot \left[1 + \left(\frac{K - 1}{2}\right) \cdot Ma3d^{2}\right]^{h}$$

$$Ma3 = Ma3d$$

$$p_2 = \text{variable}$$

$$Pt3 = p_2 \cdot Pt3d$$

$$m3 = m3d \cdot \frac{Pt3}{Pt3d}$$

$$c = \frac{K}{K - 1}$$

$$c1 = \frac{K - 1}{2}$$

$$c2 = p^{\left[\frac{K - 1}{K}\right]}$$

$$c3 = p^{\left[\frac{K-1}{K}\right]} - 1$$

$$c4 = K \cdot R \cdot Tt1$$

$$c5 = \frac{A1}{Tt1^{0.5}} \cdot \left[\frac{K}{R}\right]^{0.5}$$

$$c6 = \frac{A2}{Tt2^{0.5}} \cdot \left[\frac{K}{R}\right]^{0.5}$$

$$Ma2 = \left[\frac{p^{\left(\frac{K-1}{K}\right)} - 1}{\frac{K-1}{2}} + p^{\left(\frac{K-1}{K}\right)} \cdot Ma1^{2}\right]^{0.5}$$

$$Pt1 = \left[\frac{R}{K} \cdot Tt2\right]^{0.5} \cdot \left[\frac{m3}{p \cdot A2 \cdot \left(1 + c1 \cdot \left[\frac{c3}{c1} + c2 \cdot Ma1^{2}\right]\right)^{h} \cdot \left(\frac{c3}{c1} + c2 \cdot Ma1^{2}\right)^{0.5} + A1 \cdot (1 + c1 \cdot Ma1^{2})^{h} \cdot Ma1}\right]$$

$$P1 = \frac{Pt1}{(1 + c1 \cdot Ma1^2)^c}$$

$$m1 = Pt1 \cdot c5 \cdot Ma1 \cdot (1 + c1 \cdot Ma1^2)^h$$

$$m2 = p \cdot Pt1 \cdot c6 \cdot Ma2 \cdot (1 + c1 \cdot Ma2^2)^h$$

$$v1 = Ma1 \cdot \left[\frac{c4}{1 + c1 \cdot Ma1^2}\right]^{0.5}$$

$$v2 = Ma2 \cdot \left[\frac{c4}{1 + c1 \cdot Ma2^2}\right]^{0.5}$$

$$P3 = \frac{Pt3}{(1 + c1 \cdot Ma3^2)^c}$$

$$v3 = Ma3 \cdot \left[\frac{c4}{1 + c1 \cdot Ma3^2}\right]^{0.5}$$

$$Ac = Pt1 \cdot c5 \cdot Ma1 \cdot (1 + c1 \cdot Ma1^2)^h \cdot Ma1 \cdot \left[\frac{c4}{1 + c1 \cdot Ma1^2}\right]^{0.5}$$

$$Bc = p \cdot Pt1 \cdot c6 \cdot Ma2 \cdot (1 + c1 \cdot Ma2^2)^h \cdot Ma2 \cdot \left[\frac{c4}{1 + c1 \cdot Ma2^2}\right]^{0.5}$$

$$Cc = \left[\left(\frac{R}{K} \cdot Tt2\right)^{0.5} \cdot \left(\frac{m3}{\dfrac{p \cdot A2 \cdot \left[1 + c1 \cdot \left(\dfrac{c3}{c1} + c2 \cdot Ma1^2\right)\right]^h \cdot \left[\dfrac{c3}{c1} + c2 \cdot Ma1^2\right]^{0.5} + A1 \cdot (1 + c1 \cdot Ma1^2)^h \cdot Ma1}{(1 + c1 \cdot Ma1^2)^c}} - P3\right)\right] \cdot A3$$

$$Dc = m3 \cdot v3$$

$$0 = Ac + Bc - Dc + Cc$$

THIS PAGE INTENTIONALLY LEFT BLANK

APPENDIX D TEMPERATURE DISTORTION (EES CODE)

$$m4d = 4.381$$

$$Pt4d = 76803$$

$$D4 = \frac{11}{12 \cdot 3.28}$$

$$A4 = \pi \cdot \frac{D4^{2}}{4}$$

$$K = 1.4$$

$$R = 287$$

$$cp = R \cdot \left[\frac{K}{K - 1}\right]$$

$$Td = 29.4$$

$$Tt4d = Td + 273.15$$

$$Pta = 101325$$

$$Tta = Tt4d$$

$$h = \frac{-(K + 1)}{2 \cdot (K - 1)}$$

$$m4d = Pt4d \cdot \frac{A4}{Tt4d^{0.5}} \cdot \left[\frac{K}{R}\right]^{0.5} \cdot Ma4d \cdot \left[1 + \left(\frac{K - 1}{2}\right) \cdot Ma4d^{2}\right]^{h}$$

$$Pt3d = Pt4d$$

$$Tt3d = Tt4d$$

$$D3 = \frac{18}{12 \cdot 3.28}$$

$$A3 = \frac{D3^{2}}{4} \cdot \pi$$

$$m3d = m4d$$

$$m3d = Pt3d \cdot \frac{A3}{Tt3d^{0.5}} \cdot \left[\frac{K}{R}\right]^{0.5} \cdot Ma3d \cdot \left[1 + \left(\frac{K - 1}{2}\right) \cdot Ma3d^{2}\right]^{h}$$

$$a = 0.08$$

$$A2 = a \cdot A3$$

$$A2 = A1 \cdot \left[\frac{a}{1 - a}\right]$$

$$Tt1 = Tt4d$$

$$t = Tratio$$

$$Tt2 = t \cdot Tt1$$

$$L = \frac{1 - a}{a}$$

$$Tt3 = \left[\frac{t}{t^{0.5} \cdot L + 1} + t^{0.5} \cdot \left(\frac{L}{t^{0.5} \cdot L + 1}\right)\right] \cdot Tt1$$

$$n = Variable$$

$$\frac{Pt3}{Pt4d} = n$$

$$m3 = m4d \cdot \left[\frac{Tt4d}{Tt3}\right]^{0.5} \cdot n$$

$$m3 = Pt3 \cdot \frac{A3}{Tt3^{0.5}} \cdot \left[\frac{K}{R}\right]^{0.5} \cdot Ma3 \cdot \left[1 + \left(\frac{K - 1}{2}\right) \cdot Ma3^{2}\right]^{h}$$

$$m1 = t^{0.5} \cdot \left[\frac{L}{t^{0.5} \cdot L + 1}\right] \cdot m3$$

$$m3 = m2 + m1$$

$$Tt3 = T3 \cdot \left[1 + \left(\frac{K - 1}{2}\right) \cdot Ma3^{2}\right]$$

$$v3 = Ma3 \cdot (K \cdot R \cdot T3)^{0.5}$$

$$Pt3 = P3 \cdot \left[1 + \left(\frac{K - 1}{2}\right) \cdot Ma3^{2}\right]^{b}$$

$$b = \frac{K}{K - 1}$$

$$0 = \frac{m1 \cdot Ma1 \cdot (K \cdot R \cdot Tt1)^{0.5} + m2 \cdot Ma1 \cdot (K \cdot R \cdot Tt2)^{0.5}}{\left[1 + \left(\frac{K-1}{2}\right) \cdot Ma1^{2}\right]^{0.5}} - m3 \cdot v3 + A3 \cdot \left[\frac{\frac{m1}{A1} \cdot \left(R \cdot \frac{Tt1}{K}\right)^{0.5}}{Ma1 \cdot \left(\left[1 + \left(\frac{K-1}{2}\right) \cdot Ma1^{2}\right]^{(h+b)}\right)} - P3\right]$$

$$Pt1 = \frac{\frac{m1}{A1} \cdot \left[R \cdot \frac{Tt1}{K}\right]^{0.5}}{Ma1 \cdot \left[1 + \left(\frac{K-1}{2}\right) \cdot Ma1^{2}\right]^{h}}$$

$$Pt1 = P1 \cdot \left[\left(1 + \left[\frac{K-1}{2}\right] \cdot Ma1^{2}\right)^{\left(\frac{K}{K-1}\right)}\right]$$

$$Ma2 = Ma1$$

$$R2 = ((K+1) \cdot (2 + (K-1) \cdot Ma2^{2})) \cdot \frac{Ma2^{2}}{(1 + K \cdot Ma2^{2})^{2}}$$

$$R2 = t \cdot Ra$$

$$Ra = ((K+1) \cdot (2 + (K-1) \cdot Maa^{2})) \cdot \frac{Maa^{2}}{(1 + K \cdot Maa^{2})^{2}}$$

$$F2 = \left[\frac{K+1}{1 + K \cdot Ma2^{2}}\right] \cdot \left[\left(\frac{2 + (K-1) \cdot Ma2^{2}}{K+1}\right)^{\left(\frac{K}{K-1}\right)}\right]$$

$$Fa = \left[\frac{K+1}{1 + K \cdot Maa^{2}}\right] \cdot \left[\left(\frac{2 + (K-1) \cdot Maa^{2}}{K+1}\right)^{\left(\frac{K}{K-1}\right)}\right]$$

$$Pt2 = Pt1$$

$$g = \frac{F2}{Fa}$$

$$Tt2 = Tta + \frac{q}{cp}$$

$$Qj = q \cdot m2$$

$$\frac{Pt2}{Pta} = j$$

$$T2 = \frac{Tt2}{1 + \left[\frac{K - 1}{2}\right] \cdot Ma2^{2}}$$

$$v2 = Ma2 \cdot (K \cdot R \cdot T2)^{0.5}$$

$$T1 = \frac{Tt1}{1 + \left[\frac{K - 1}{2}\right] \cdot Ma1^{2}}$$

$$v1 = Ma1 \cdot (K \cdot R \cdot T1)^{0.5}$$

APPENDIX E INLET VELOCITY RATIO

A. PRESSURE DISTORTION

In this case,

$$Tt_1 = Tt_2 \tag{1}$$

$$P_1 = P_2 \tag{2}$$

and

$$Pt_1 = \pi Pt_2 \tag{3}$$

From the definition of stagnation temperature,

$$V_2 = V_1\left[\frac{Tt_2 - T_2}{Tt_1 - T_1}\right]^{0.5} \tag{4}$$

Since $T_2 = Tt_2\left(\frac{P_2}{Pt_2}\right)^{\frac{(\gamma-1)}{\gamma}}$, and $T_1 = Tt_1\left(\frac{P_1}{Pt_1}\right)^{\frac{(\gamma-1)}{\gamma}}$ (5)

using equations (1), (2), (3) and (5) in equation (4),

$$V_2 = V_1\left[\frac{2}{(\gamma-1)M_1^{\,2}}\left(1-\frac{1}{\pi^{\frac{(\gamma-1)}{\gamma}}}\right)+1\right]^{1/2} \tag{6}$$

Then, from Equation (6), the minimum value of π (when $V_2 = 0$) is given by

$$\pi_{\min} = \left(1+\frac{(\gamma-1)}{2}M_1^{\,2}\right)^{\frac{-\gamma}{(\gamma-1)}} = \frac{P_1}{Pt_1} \tag{7}$$

B. TEMPERATURE DISTORTION

In this case,

$$Pt_1 = Pt_2 \tag{8}$$

$$Tt_1 = \tau Tt_2 \tag{9}$$

and

$$P_1 = P_2 \tag{10}$$

Since, from equations (8) and (10),

$$\frac{Pt_1}{P_1} = \frac{Pt_2}{P_2} \tag{11}$$

then $M_1 = M_2$ and

$$\frac{Tt_1}{T_1} = \frac{Tt_2}{T_2} \tag{12}$$

Re-writing equation (4) as

$$V_2 = V_1 \left[\left(\frac{Tt_2}{Tt_1} \right) \left(\frac{1 - \frac{T_2}{Tt_2}}{1 - \frac{T_1}{Tt_1}} \right) \right]^{0.5} \tag{13}$$

and using equation (12), then

$$V_2 = V_1 \sqrt{\tau} \tag{14}$$

LIST OF REFERENCES

1. Donelson S. and Briggs T. JSF team probes steam catapult environment, www.dcmilitary/navy/mil, February 6, 2003.

2. SAE – AIR 1419 (1983) "Gas turbine engines, inlet total-pressure-distortion consideration for".

3. SAE ARD50015 (1991) Aerospace resource document.

4. O' Brien J.M., Transonic Compressor Test Rig Rebuild and Initial Results with the Sanger Stage, MS Thesis, Naval Postgraduate School, Monterey, California, June 2000.

5. Sanger, N. L., Design of a Low Aspect Ratio Transonic Compressor Stage Using CFD Techniques, Journal of Turbomachinery, Vol. 118, 1996.

6. Hobson, G.V., Gannon, A.J. and Shreeve, R.P., A Transonic Compressor Stage: Part 1 Experimental Results, ASME Paper GT2004-53923, Turbo Expo 2004, Vienna, Austria, June 2004.

7. Gannon, A.J., Hobson, G.V. and Shreeve, R.P., A Transonic Compressor Stage: Part 2 CFD Simulation, ASME Paper GT2004-53927, Turbo Expo 2004, Vienna, Austria, June 2004.

8. CFD-GEOM Version 2004.0.1.14, CFD Research Corporation, Huntsville, Alabama.

9. CFD-VIEW Version 2004, CFD Research Corporation, Huntsville, Alabama.

10. CFD-ACE GUI Version 2004.0.25, CFD Research Corporation, Huntsville, Alabama.

THIS PAGE INTENTIONALLY LEFT BLANK

INITIAL DISTRIBUTION LIST

1. Defense Technical Information Center
   Ft. Belvoir, Virginia

2. Dudley Knox Library
   Naval Postgraduate School
   Monterey, California

3. Chairman, Code ME
   Department of Mechanical and Astronautical Engineering
   Naval Postgraduate School
   Monterey, California

4. Professor R.P.Shreeve, Code ME/Sf
   Department of Mechanical and Astronautical Engineering
   Naval Postgraduate School
   Monterey, California

5. Professor G.V.Hobson, Code ME/Hg
   Department of Mechanical and Astronautical Engineering
   Naval Postgraduate School
   Monterey, California

6. Associate Professor Knox Millsaps, Code ME/Mi
   Department of Mechanical and Astronautical Engineering
   Naval Postgraduate School
   Monterey, California

7. Mr Mark Klein
   Naval Air Systems Command
   NAS Patuxent River, Maryland

8. Mr. Ravi Ravindranath
   Naval Air Systems Command
   NAS Patuxent River, Maryland

9. Mr. Dan Popgoshev
   Naval Air Systems Command
   NAS Patuxent River, Maryland

10. GEN B2-III
Hellenic General Staff of the Navy
Athens, Greece